



City Research Online

City, University of London Institutional Repository

Citation: Le, B. T., Nguyen, T. T. T., Divall, S. & Davies, M. C. R. (2023). A study on large volume losses induced by EBPM tunnelling in sandy soils. *Tunnelling and Underground Space Technology*, 132, 104847. doi: 10.1016/j.tust.2022.104847

This is the accepted version of the paper.

This version of the publication may differ from the final published version.

Permanent repository link: <https://openaccess.city.ac.uk/id/eprint/29167/>

Link to published version: <https://doi.org/10.1016/j.tust.2022.104847>

Copyright: City Research Online aims to make research outputs of City, University of London available to a wider audience. Copyright and Moral Rights remain with the author(s) and/or copyright holders. URLs from City Research Online may be freely distributed and linked to.

Reuse: Copies of full items can be used for personal research or study, educational, or not-for-profit purposes without prior permission or charge. Provided that the authors, title and full bibliographic details are credited, a hyperlink and/or URL is given for the original metadata page and the content is not changed in any way.

City Research Online:

<http://openaccess.city.ac.uk/>

publications@city.ac.uk

A study on large volume losses induced by EBPM tunnelling in sandy soils

Authors

B. T. Le, T. T. T. Nguyen, S. Divall, M. C. R. Davies

Abstract

Tunnelling-induced ground surface settlements can be described by a Gaussian distribution curve with two key factors; the displacement trough width and the volume loss. In most cases the volume losses are well-controlled with maximum settlements less than the allowable limits. However, there have been reports showing abnormally large ground surface settlement, in sandy soil, induced by Earth Pressure Balance Tunnel Boring Machines (EPB TBMs). This research reports field data obtained during the construction of the Metro Line 1 Ben Thanh – Suoi Tien Tunnels in Ho Chi Minh city, Vietnam. Data include ground settlement measurements, the geotechnical conditions and TBM operation parameters. The results show that in locations where large settlements had occurred there were common characteristics of high liquefaction index, large excess pore pressure and abnormally large tail void grouting. A novel equation is suggested to describe the relationship between the volume loss and the liquefaction potential index. This has been calculated using simple and commonly available geotechnical parameters for use in practice as an indicator for potentially large settlements caused by EBP TBM tunnelling in sandy soils.

Keywords

EPB TBM; Ground movements; Tunnelling; Case study

LIST OF SYMBOLS AND ABBREVIATION

α	Peak ground acceleration		into account the effect of grain size
$\Delta\sigma_F$	Change in face pressure		
Δu	Change in pore-water pressure	PL	Liquefaction potential index
ε_a	Axial strain	p'	Mean effective stress
σ_F	Pressure at the TBM face	p'_0	Initial mean effective stress
σ'_h	Horizontal effective stress	q	Deviatoric stress
σ'_{h0}	Initial horizontal effective stress	R	Dynamic shear strength ratio
σ_v	Vertical total stress	R_L	Cyclic triaxial strength ratio
σ'_v	Vertical effective stress	SSL	Steady state line
σ'_{v0}	Initial vertical effective stress	s	Ground surface settlement
γ_d	Reduction coefficient	s_{max}	Maximum ground surface settlement
$C_1 \& C_2$	Coefficients considering the fine contents F_c	TBM	Tunnel Boring Machine
C_w	Coefficient defined according to the type of the seismic motion	u	Pore-water pressure
D	Excavation diameter	V_{exc}	Volume of the excavation area
D_{50}	Mean grain diameter	V_L	Volume loss
D_r	Relative density	$V_{L(x)}$	Volume loss when the EPBM was at a distance x to the monitoring section
EPBM	Earth Pressure Balance Machine	$V - Grout$	Volume of tail void grout per ring
F	Safety rate to liquefaction	V_S	Volume of the settlement trough
FLS	Flow liquefaction surface	V_t	Volume of ground loss in the region close to the tunnel
FL	Factor of safety to liquefaction	$V - Void$	Volume of tail void per ring
F_c	Fines content	$w(z)$	Weight function in accordance with depth z
i	Horizontal distance to the point of inflexion	x	Distance from TBM face to monitoring section (m)
K	Dimensionless settlement trough width parameter	y	Distance from the tunnel centre-line
K_0	Earth pressure coefficient at rest	z	Depth from the ground surface
L	Seismic shear stress ratio	z_0	Depth from the ground surface to tunnel axis level
N	Raw SPT count at site		
N_1	Normalised N-value		
N_a	Amended N-value taking		

1 **INTRODUCTION**

2 Tunnel construction inevitably causes ground movements (**Figure 1**) which, potentially, can result in
3 severe damage to surrounding buildings and buried infrastructure. Therefore, accurate prediction of
4 tunnelling-induced ground deformations is of essential for safe tunnel excavation.

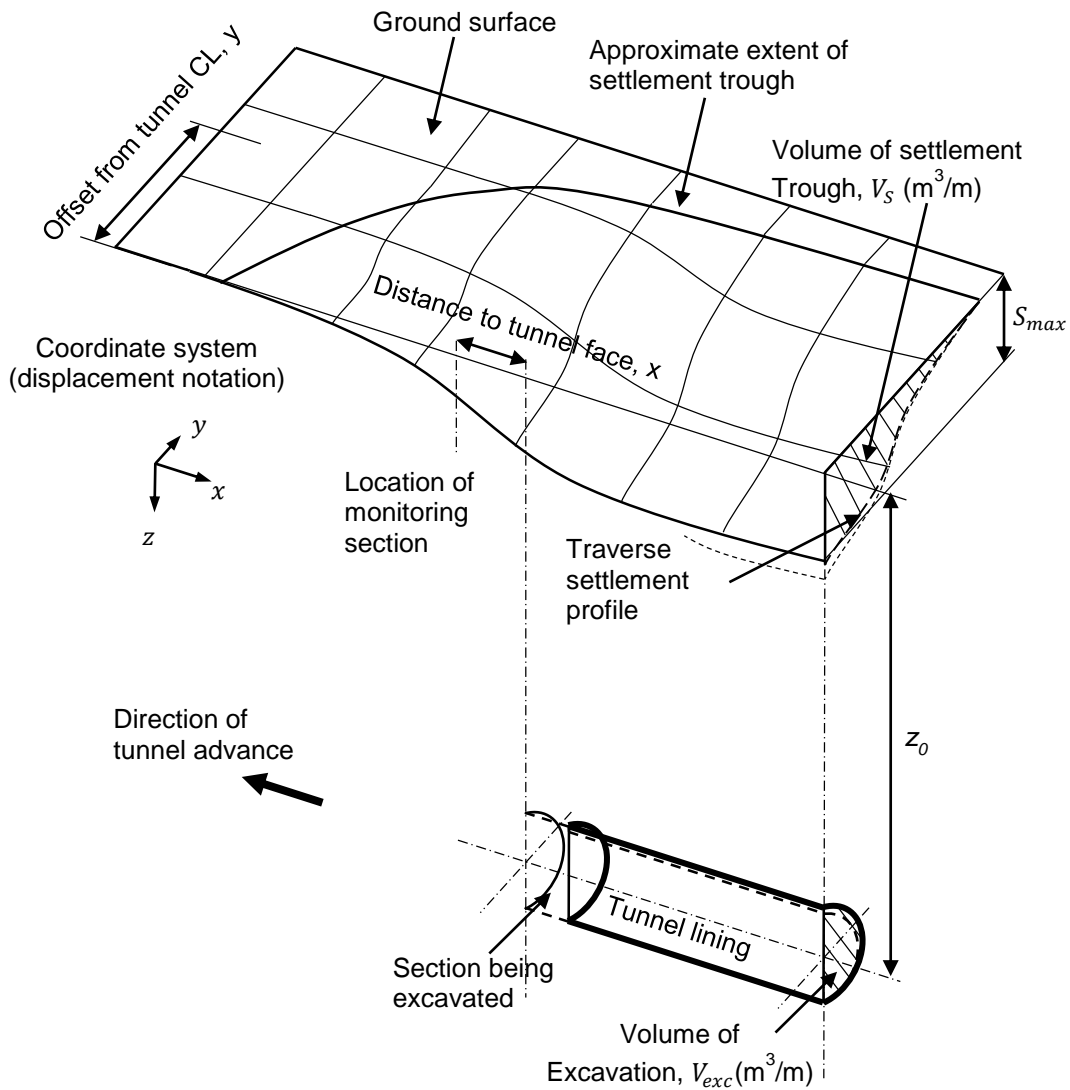


Figure 1. Idealisation of tunnelling induced soil displacement (after Le and Taylor, 2018).

5
6 By investigating the field data from case studies, previous research including many studies (Dimmock,
7 2003; Mair & Taylor, 1997; Nyren, 1998; Peck, 1969; Schmidt, 1969; Shirlaw et al., 2003; Sugiyama et
8 al., 1999; Wan et al., 2017a) have indicated that the ground surface transverse settlement, s , has the
9 shape of a Gaussian distribution curve, as shown in **Figure 2**, and can be described by Equation 1 as
10 below;

$$s = s_{max} \exp\left(\frac{-y^2}{2i^2}\right) \quad (1)$$

$$s_{max} = \frac{V_s}{\sqrt{2\pi}i}; \quad (2)$$

11

12 where s_{max} is the maximum settlement and normally occurs above the centre-line of the tunnel;

13 V_s is the volume of the transverse surface settlement trough (**Figure 2**);

14 y is the distance from the tunnel centre-line;

15 i is the horizontal distance to the point of inflexion.

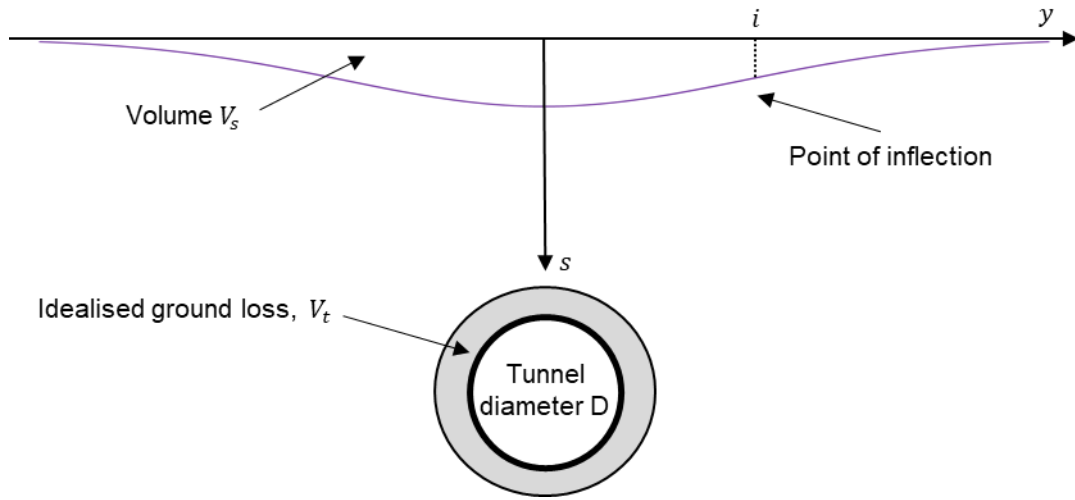


Figure 2. Ground surface settlement trough (Not to scale).

16

17 The ground loss, V_t , is the amount of ground lost in the region close to the tunnel (Franza et al., 2019;

18 Mair and Taylor, 1997). When tunnelling in clayey soils, ground movements normally undergo undrained

19 conditions (constant volume) hence $V_s = V_t$. For tunnelling in coarse grain soils, ground deformations

20 are usually under drained conditions, that can result in dilation of the soil, therefore it is highly likely that

21 $V_s < V_t$. Regardless of soil type, Mair & Taylor (1997) suggested that it is convenient to express the

22 volume loss, V_L , in term of the ratio of the volume of the settlement trough, V_s , with the volume of the

23 excavation area, V_{exc}

$$V_s = V_L \times V_{exc}; \quad (3)$$

$$V_{exc} = \pi \frac{D^2}{4}; \quad (4)$$

$$i = Kz_0 \quad (5)$$

24 where D is the excavation diameter;

25 K is the dimensionless settlement trough width parameter;

26 z_0 is the depth from the ground surface to tunnel axis level.

27 Combining the Equations 2, 3, 4, 5 gives;

$$s = 0.313 \frac{V_L D^2}{K z_0} \exp\left(\frac{-y^2}{2(K z_0)^2}\right) \quad (6)$$

28

29 At a specific location, the diameter, D , and depth, z_0 , of the tunnel, the distance from the tunnel centre-
30 line, y , are known leaving the values of the settlement trough width parameter, K , and the volume loss,
31 V_L , to be selected for estimation of the ground surface settlement due to tunnelling. The parameter K
32 depends mainly on the type of soil (O'Reilly & New, 1982). This value can range from 0.2 to 0.7 and
33 influences the width of the overall settlement trough (Mair, 2008; Mair & Taylor, 1997). The volume loss
34 dictates the magnitude of tunnelling-induced ground settlement (Vu et al., 2016). The volume loss
35 magnitude normally ranges from 0.2% to 1% (Wongsaroj et al., 2006; Dimmock, 2003; Wan et al.,
36 2017a; Islam & Iskander, 2021) and in some cases it can be larger than 2% (Shirlaw et al., 2003; The
37 British Tunnelling Society and The Institution of Civil Engineers, 2005) but is mainly dependent on the
38 ground conditions and tunnelling techniques. The latter factor regarding Earth Pressure Balance
39 Machine (EPBM) tunnelling technology is described in the next section followed by an explanation of
40 the resulting volume loss induced during the tunnel construction stages.

41

42 **EPBM TUNNELLING**

43 The key aspects of an EPBM are depicted in **Figure 3**. The cutterhead excavates the soil in front of the
44 tunnel which then passes into the chamber. Conditioning agents, usually bentonite, foam or polymers,
45 are injected into the plenum (chamber) to mix with the excavated soil to form high viscosity fluid or
46 plasticised spoil (Chapman et al., 2018; Dias & Bezuijen, 2015; Mair, 2008). The resulting plasticised
47 spoil allows easy extraction of the excavated materials. This low water permeability spoil also forms a
48 suitable medium to transfer pressure from the chamber to the tunnel face that allows pressure control
49 in the chamber head (Chapman et al., 2018). An Archimedean screw (screw conveyor) is used to extract
50 the plasticised spoil from the chamber in a controlled manner to maintain stable pressure in the chamber
51 (Chapman et al., 2018). In some cases, conditioning agents are also introduced at the cutterhead and
52 the screw conveyor (Mair, 2008).

53

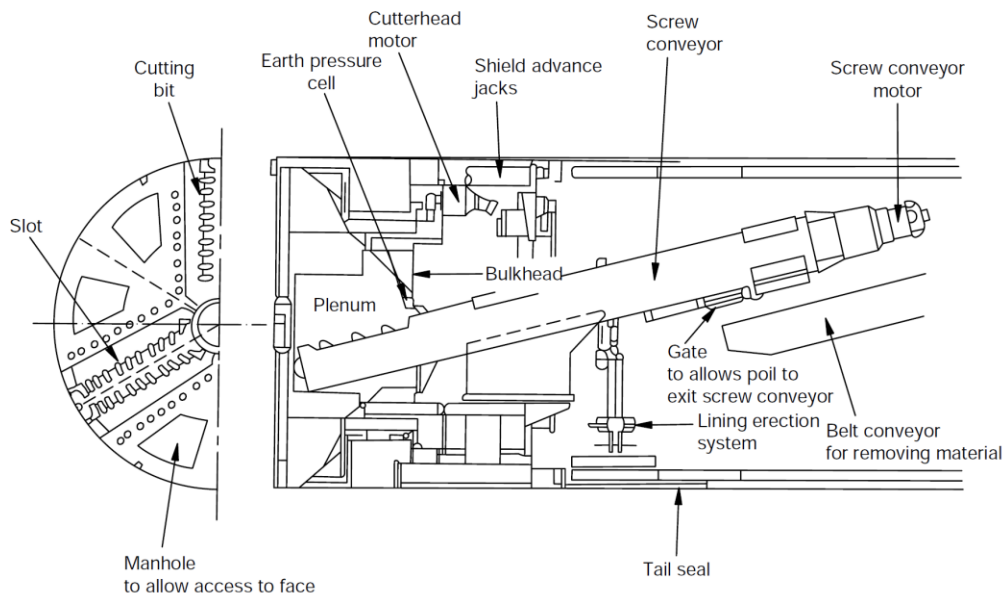


Figure 3. Main components of Earth pressure balance tunnelling machine (Chapman et al., 2018).

54 The pressure in the chamber can be regulated to provide support, together with the thrust from the
 55 machine advancing jacks to the cutterhead, to substantially balance against the soil and pore-water
 56 pressures. The screw conveyor plays an important role in controlling the chamber pressure. If the
 57 excavation rate is steady, reducing the conveyor speed increases the chamber pressure whereas
 58 increasing the conveyor speed reduces the chamber pressure.

59

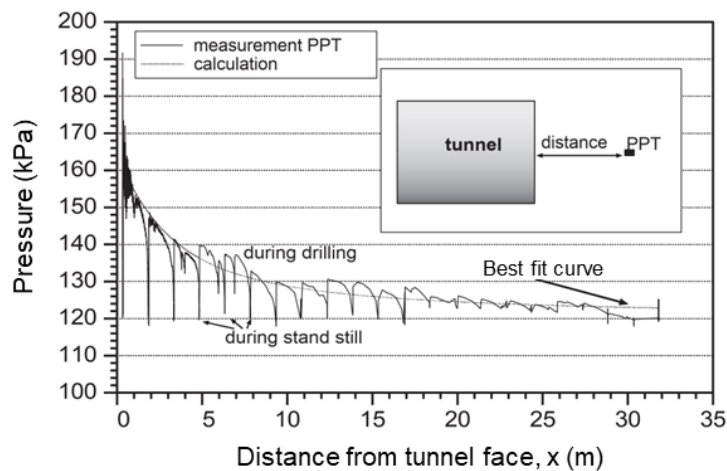
60 The force provided by the jacks is required to overcome the friction on the shield skin together with the
 61 force exerted by the pressure in the chamber and drag of the trailing gear (Japan Society of Civil
 62 Engineers, 2016; Standing & Selemetas, 2013) in order to thrust the machine forward. When the TBM
 63 stops, the force provided by the jacks reduces to a level that is required to balance the pressure exerted
 64 by the face.

65

66 **CHANGES IN PORE-WATER PRESSURE DURING TBM TUNNELLING**

67 The main concern of the project owners and contractors in tunnelling projects are the induced ground
 68 movements, buried services and building deformations. However, well reported measurements of the
 69 pore-water pressure changes resulting from TBM tunnelling is limited in the literature (Aime et al., 2004;
 70 Bezuijen et al., 2017; Broere, 2001; Dias & Bezuijen, 2015; Jin et al., 2022; Kaalberg et al., 2014; Liu et
 71 al., 2014; Shi et al., 2021; Wan et al., 2019) .

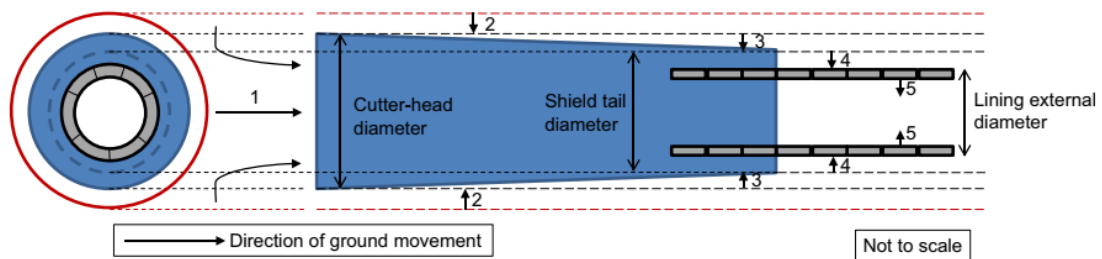
72 **Figure 4** illustrates typical field pore-water pressure changes, recorded by an in-situ pore pressure
 73 transducer (PPT), during tunnel excavation by a slurry TBM in sandy soils (Bezuijen, 2006; Kaalberg et
 74 al., 2014). The PPT was pre-installed in the tunnel axis and was destroyed by the TBM upon arriving.
 75 Therefore, the measured data is only available until the TBM's face reached the PPT location. The
 76 magnitude of the excess pore-water pressure measured by the PPT increases as the TBM approached
 77 towards the monitoring section (Aime et al., 2004; Xu & Bezuijen, 2019, 2018). It can be seen that the
 78 cyclic loading and unloading when the TBM advances and stops resulted in peak and low values of
 79 excessive pore pressure, respectively, i.e. excess pore pressures were measured in front of the TBM
 80 during drilling and these decreased to hydrostatic pressure when the drilling stopped.
 81



82 Figure 4. Measured excess pore pressure in front of a TBM in sandy soil (after Bezuijen, 2006).

83 **VOLUME LOSS INDUCED BY TBM TUNNELLING**

84 The tunnel excavation process causes changes to the stress state and pore-water pressure in soils
 85 which results in ground movements. Leca et al. (2007) and Wan et al. (2017b) categorise volume loss,
 86 induced by TBM tunnelling, into 5 components as depicted in **Figure 5**.



87
 88 Figure 5. Illustration on components of volume loss (Wan et al., 2017b).

- 89
- 90 - Component 1 – Face movement: occurs when the support pressure provided by the tunnel face
 - 91 is less than the ground stresses. Therefore, it is critical to maintain substantial pressure at the

92 tunnel face to minimise the effect of this component. However, using excessive support
93 pressure also results in a higher effective stress in the ground just before the cutting wheel and
94 leads to lower production and higher necessary torque on the cutting wheel. In addition,
95 excessive support pressure may cause 'blow out'. In some cases, contractors were discouraged
96 from using a face pressure larger than 120% of the total overburden pressure (Shirlaw et al.,
97 2003). Long stoppages of TBM with the head empty or partially empty, mainly for maintenance
98 or TBM problems, can cause reduction in face pressure and hence increase in settlement at
99 tunnel face (Biggart & Sternath, 1996; Shirlaw et al., 2003). In addition, unforeseen obstructions
100 in ground, unexpected mixed face soil conditions also contribute to ground movements (Clough
101 and Leca, 1993; Shirlaw, 2016; Tóth et al., 2013; Vergara & Saroglou, 2017) .

102 - Components 2 and 3 – Movement around the shield body: in order to enable ease of the
103 machine advancing, the diameter of the cutter head is larger than the TBM shield (component
104 2) and in some cases the shield has the cone shape (component 3) (Biggart & Sternath, 1996;
105 Kavvadas et al., 2017; Liu et al., 2017; Wan et al., 2017b). These two factors result in voids
106 between the excavated soil and the shield skin. Under gravity, soils around the shield have the
107 tendency to settle and close the void. However, it has been reported that the gap between the
108 soil and the TBM shield can be reduced by the tail void grout, that also flows over the smaller
109 diameter part of the shield, resulting in less volume loss (Bezuijen & Bakker, 2009, 2007).

110 - Component 4 – Tail void closure: as the tunnel linings are erected inside the machine, their
111 diameter is smaller than that for the cutter head and the TBM shield. That in turn creates a void
112 between the final tunnel lining with the excavated soil. In order to minimise the closing up of the
113 void to minimise the consequential settlement, tail void grouting is injected immediately to fill
114 that cavity (Do et al., 2021; Liu et al., 2021). Because of the ground permeation and over-cutting,
115 the actual volume of the injected grout may range from 130–170% of the theoretical tail void
116 volume and sometimes higher in gravel soils (Japan Society of Civil Engineers, 2016). Liu et al.
117 (2017) and Vonk (2020) observed that higher grout volume leads to smaller settlement. Liu et
118 al. (2020) suggested that for shallow tunnels, the ratio should not exceed 145% to avoid
119 penetration of the grout to the ground surface.

120 - Component 5 – Lining deformation under soils and pore-water stresses, and long-term ground
121 settlement due to consolidation. This component is not considered in this paper.

122

123 With strict requirements imposed by the project owners, the common threshold for V_L in practice is
 124 normally less than 1% (Wongsaroj et al., 2006) and for congested urban environments the threshold
 125 can be less than 0.5%. This paper aims to gain a better insight into prediction of abnormally large
 126 settlement by analysing the field data including the geotechnical conditions, geometry and arrangement
 127 of the tunnels, the operation parameters of the EPB TBM in the following case study.

128

129 **THE CASE STUDY**

130 The twin tunnels, in this research, form part of metro line 1 Ben Thanh – Suoi Tien in Ho Chi Minh city,
 131 Vietnam (Le et al., 2021). These 781m long twin tunnels were the first tunnels excavated by EPBM in
 132 Vietnam. The plan and longitudinal profiles of the tunnels, including the soil conditions along the routes,
 133 are depicted in **Figure 6**. The East Bound (EB) tunnel was constructed from 26th May 2017 to 31st
 134 October 2017. The EPBM was launched from Bason station (chainage 1586m) and excavated towards
 135 the Opera House station (chainage 805m). The TBM was then dismantled and transported back to
 136 Bason station for West Bound (WB) tunnel excavation. The WB tunnel was constructed from 26th
 137 January 2018 to 29th June 2018 (Le et al., 2020). **Figure 7 a, b** present the advance rate of the TBM in
 138 EB and WB tunnels, respectively. At the beginning of the excavation from chainage 1586m, an initial
 139 drive of approximately 80m was carried out at a slow rate (**Figure 7**). The EPBM was then stopped at
 140 around chainage 1500m for a review of the operational parameters before continuing the main drive for
 141 the rest of the route.

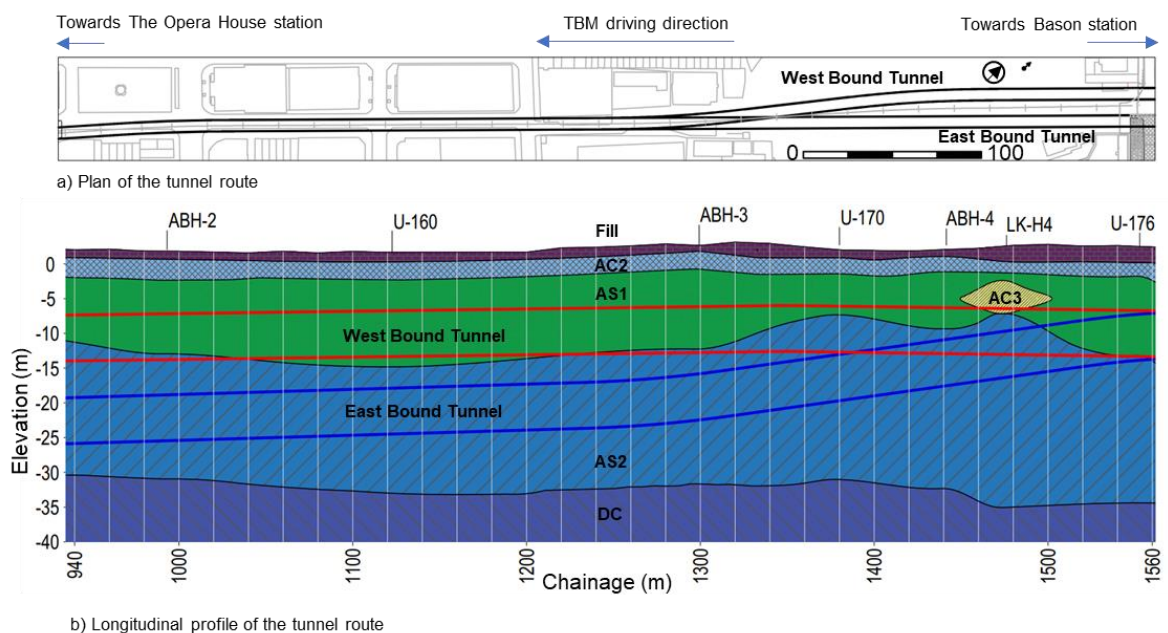
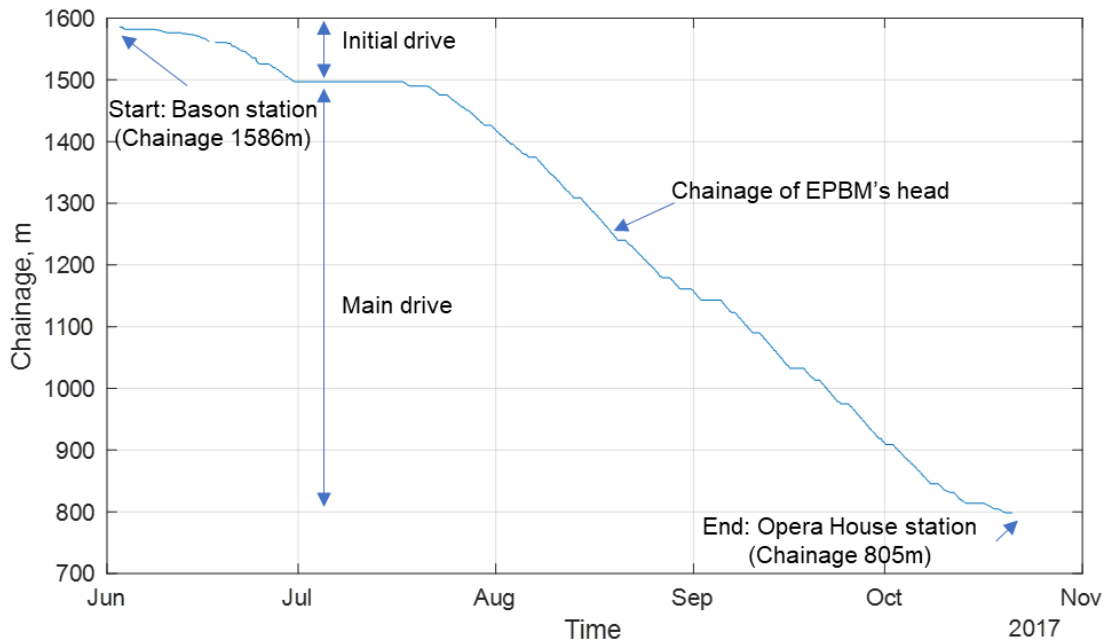
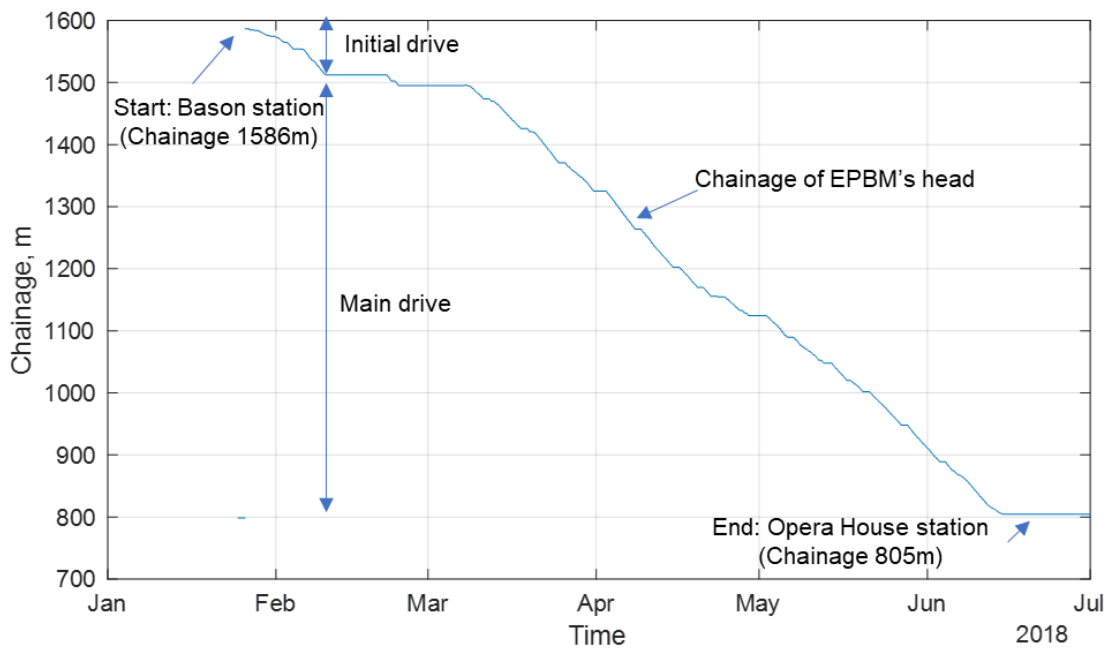


Figure 6. Plan and longitudinal profile of the tunnel route.



a) TBM advance rate in EB tunnel



b) TBM advance rate in WB tunnel

Figure 7. TBM advance rate

142 **SITE GEOLOGY**

143 The Soil Investigation report shows that the water table is 2m below the ground surface and the soil
 144 consists of five main geological layers (**Figure 6**) as described below:

- 145 - Fill: The top soil is mainly fill materials including sand, clay, gravel, brick, concrete. At most of the
- 146 boreholes, the thickness of this layer is less than 2m. The coefficient of permeability is $k=1 \times 10^{-6} \text{m/s}$.

147 - AC2 (Alluvial clay 2): The soil material is homogenous, very soft fat CLAY, bluish grey. The layer
148 thickness varies from 0 to 4.5m with the average SPT N-value of 2. The coefficient of permeability is
149 $k=1 \times 10^{-9} \text{m/s}$.

150 - AS1 (Alluvial sand): silty fine SAND layer. In general, the soil is very loose to loose, non-homogeneous
151 to homogenous. Silt content ratio decreases with depth and changes to fine sand with silt. The layer
152 thickness varies from 3.2m to 13m with the average SPT N-value of 5. The coefficient of permeability is
153 $k=2 \times 10^{-5} \text{m/s}$.

154 - AS2 (Alluvial sand): This layer is the lowermost in alluvium deposit and above the hard clayey silt of
155 diluvium. The main component of this layer is medium to coarse SAND and the density is from medium
156 dense to dense sand with occasional loose pockets. The thickness varies from 16.9m to 27.8m with the
157 average SPT N-value of 15. The coefficient of permeability is $k=2 \times 10^{-5} \text{m/s}$.

158 - AC3 (Alluvial clay 3): The soil material is homogeneous, firm to stiff fat CLAY with sand. The thickness
159 varies from 0.5m to 7m with the average SPT N-value of 8. The coefficient of permeability is $k=10^{-9} \text{m/s}$.

160 - DC (Diluvium clay): The material consists of homogeneous, hard to very hard, weakly cemented, low
161 permeability, CLAY. The thickness varies from 2.9m to 21.1m with the average SPT N-value of 34. The
162 coefficient of permeability is $k=1 \times 10^{-8} \text{m/s}$.

163 As can be seen from **Figure 6**, most of the EB tunnel is within the sandy soil AS2 while the WB tunnel
164 is within the sandy soil AS1 and at some locations the cross-section of the tunnel encounters mixed
165 soils of AS1 and AS2.

166

167 **THE TUNNELLING MACHINE**

168 An Earth Pressure Balance Machine (EPBM) was chosen to construct the tunnel as this type of machine
169 is suitable with the sandy ground conditions. The excavation diameter and the shield body diameter are
170 6.82m and 6.79m, respectively. The length of the EPBM from the cutter face to tail is 8.5m. The tunnel
171 lining rings consist of 6 precast concrete segments including three regular, two counter key and one key
172 segments. Each section of the tunnel lining has a nominal length of 1.2m with the outer and inner
173 diameters of 6.65m and 6.05m, respectively. The machine advances forward by means of 20 hydraulic
174 jacks with a maximum combined thrust of 40,000kN applied to the erected linings to overcome the
175 friction and the face pressure. In addition, along the shield high viscosity bentonite was injected to act
176 as lubricant between the shield extrados and the surrounding soil. At the TBM tail, the void between the
177 tunnel lining extrados and the surrounding soil was filled with a two-part grout consisting of Liquid A and
178 Liquid B. Liquid A was a mix of cement, bentonite, stabilizer and water while Liquid B was a sodium

179 silicate accelerator. The two-part grout was injected via simultaneous backfill-grouting ports. The grout
180 injection volume was designed to be 130% of the theoretical tail-void volume.

181

182 There were four earth pressure gauges installed behind the cutter face to monitor the soil stresses in
183 the vicinity of the tunnel face. The key TBM operation parameters including the face pressure, volumes
184 and pressures of the bentonite at the tunnel face and along the TBM shield, volume and pressure of the
185 tail void grouting, the machine position with time, the hydraulic jack pressures, were recorded at every
186 5 seconds during the excavation. Those parameters are detailed and analysed together with the field
187 ground surface settlement in the later sections to gain better insight into the tunnelling-induced
188 behaviour of the sandy soils.

189

190 **THE MONITORING SCHEME**

191 The monitoring points, measured by precise levelling techniques, were arranged approximately
192 perpendicular to the tunnel centre-line (Le et al., 2020). At each section, there were five to eight
193 monitoring points. The ground surface vertical displacement readings were taken once a day when the
194 TBM was within -100m to -10m and twice a day when it was -10m to +40m from the monitoring sections.
195 The negative sign indicates that the TBM was approaching the section whereas the positive sign
196 indicates the TBM was leaving the monitoring section.

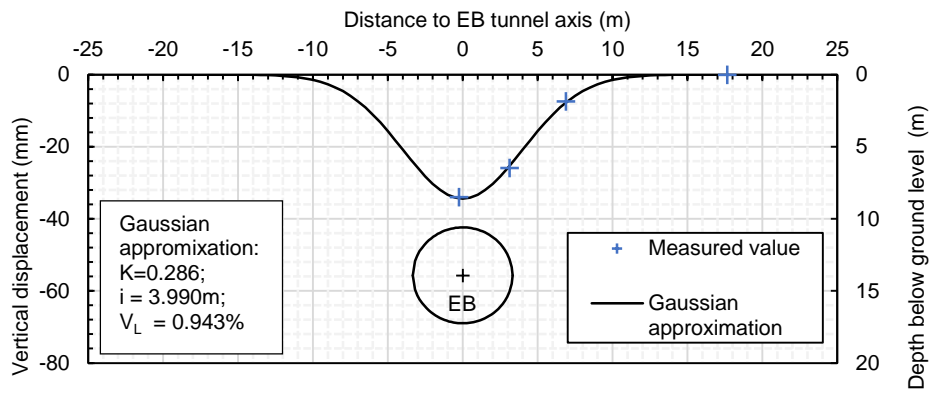
197

198 **FIELD MEASUREMENT ON GROUND SURFACE DISPLACEMENT**

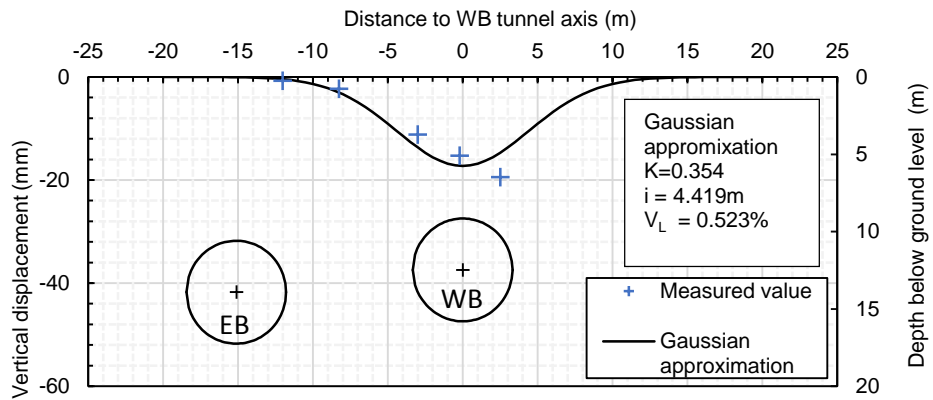
199 Previous research (Le et al., 2016; Le & Taylor, 2018; Nyren, 1998; O'Reilly & New, 1982) indicates that
200 in longitudinal direction along the tunnel centre-line, the ground surface settlement begins to develop
201 and reach a stabilised magnitude when the TBM is within the distance of x from $-z_0$ to $+z_0$, respectively.
202 In this project, the ground surface settlements due to tunnelling are calculated with the baseline when
203 the TBM was at approximately -40m to the monitoring sections which covers the range of the tunnel
204 depth of $z_0 \leq 24m$. The ground surface settlement due to tunnel construction was calculated as the
205 difference between the measured values when the TBM was at -40m and +40m to the monitoring
206 sections.

207 At some monitoring sections, there were no measurements directly above the tunnel centre-lines where
208 the largest ground vertical displacement normally occurs. Therefore, the method proposed in Jones &
209 Clayton (2013) was used to fit Gaussian approximations to available settlement data, allowing the
210 maximum ground surface vertical displacement, s_{max} , volume loss, V_L , and trough width parameter, K ,

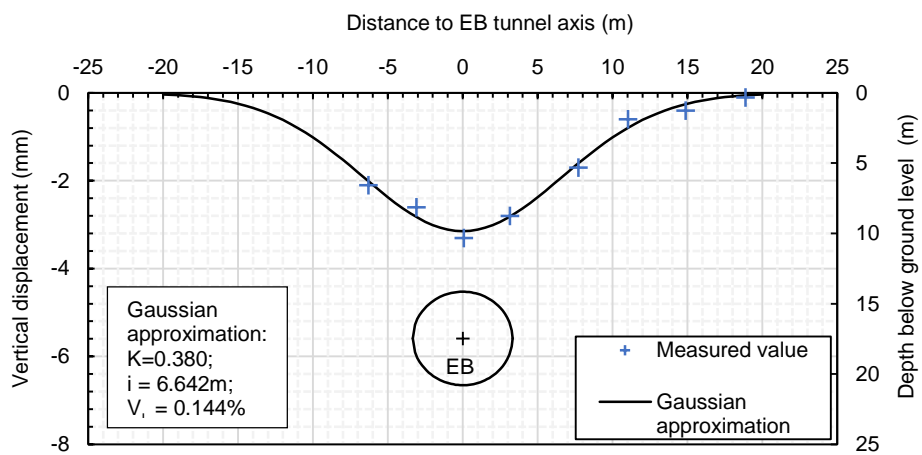
211 to be obtained. **Figure 8** presents the Gaussian approximations and corresponding parameters obtained
 212 for the EB and WB tunnels at different locations representing geometries where the tunnels were
 213 positioned in parallel, diagonal and stacked arrangements.



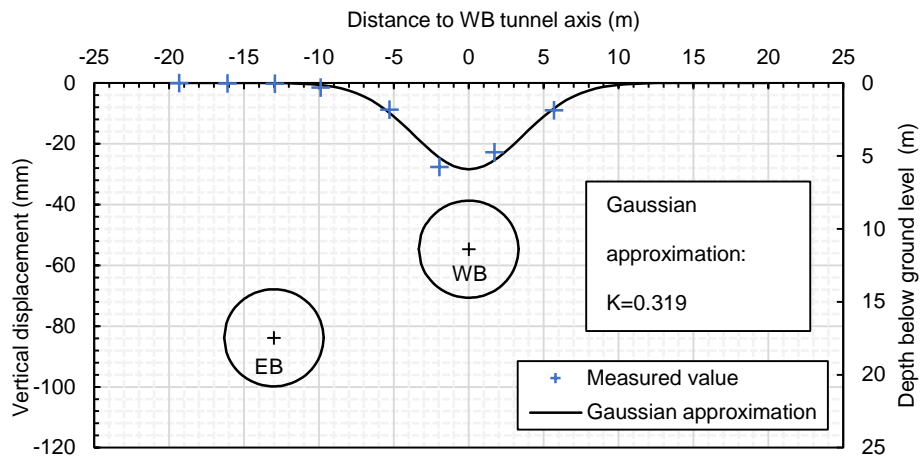
a) Ground surface vertical displacement due to EB tunnel excavation at chainage 1523m



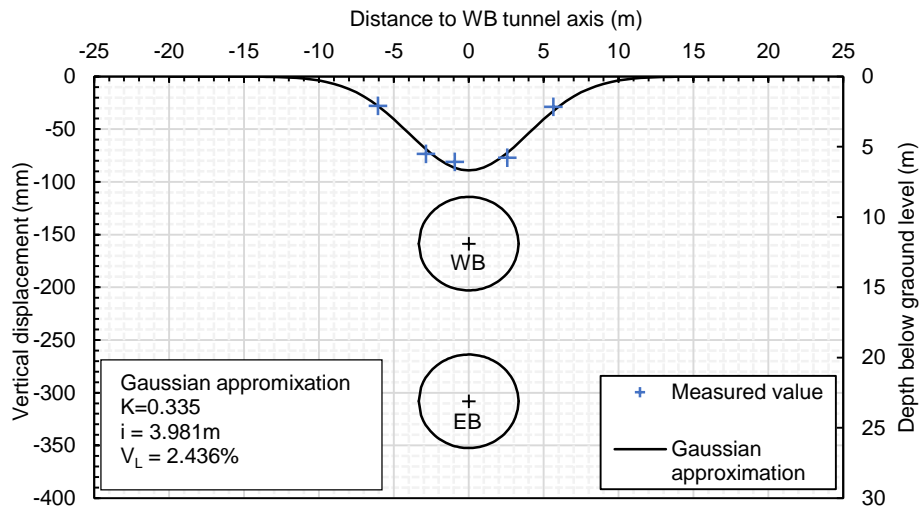
b) Ground surface vertical displacement due to WB tunnel excavation at chainage 1523m



c) Ground surface vertical displacement due to EB tunnel excavation at chainage 1403m



d) Ground surface vertical displacement due to WB tunnel excavation at chainage 1403m

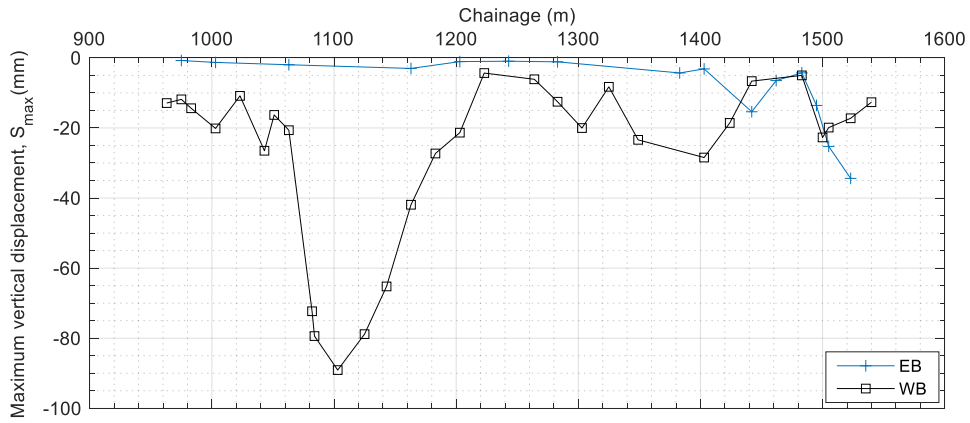


e) Ground surface vertical displacement due to WB tunnel excavation at chainage 1103m

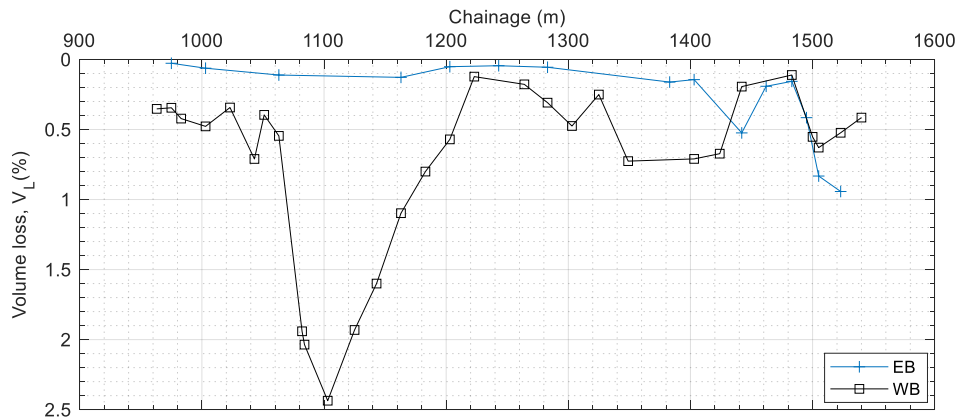
Figure 8. Ground surface settlement troughs and Gaussian approximations.

214

215 The maximum ground surface settlements and the corresponding volume losses along the tunnel route
 216 were determined and are presented in **Figure 9 a, b**, respectively.



a. Maximum ground surface settlement along the tunnel route



b. Volume loss along the route

Figure 9. Longitudinal ground surface settlement and volume loss.

217 There were some large ground surface settlements occurring especially from chainage 1080m to 1160m
 218 on the WB tunnel with the volume loss up to 2.4%. However, for the EB tunnel, the majority of the surface
 219 settlements were less than 5mm and the volume losses were less than 0.2%. There were some
 220 exceptions where values of settlements and volume losses were similar to those of the WB tunnel at
 221 chainage 1442m and 1520m where the depth of tunnel approached that of the WB tunnel. **Figure 10**
 222 depicts typical profiles of $V_{L(x)}$, volume loss when the EPBM was at a distance x to the monitoring section
 223 along the tunnel centre-line during the TBM advancement, normalised against V_L , the total volume loss.
 224 Also in this figure, is the approximation of the contribution of the volume loss components which are
 225 illustrated by the horizontal dashed lines.

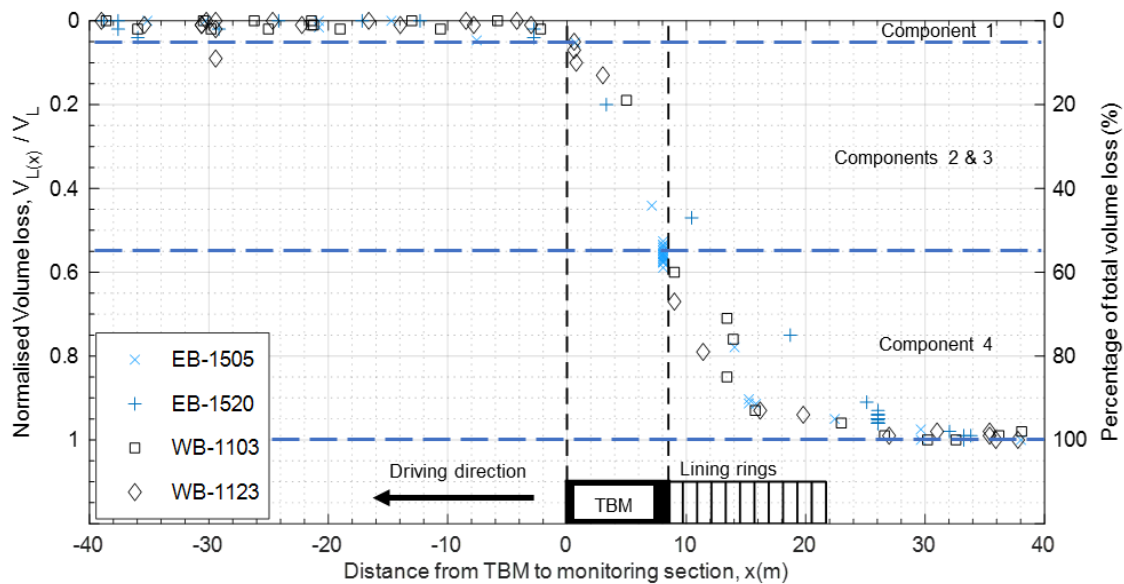


Figure 10. Typical normalised volume losses along the tunnel centre-line

226 From **Figure 10**, it can be seen that the relative contribution of volume loss components (as defined
 227 above and in **Figure 5**), in terms of percentage of the total volume loss, in the EB and WB are consistent.
 228 The component 1 contribution is negligible which only accounts for less than 5% of the total volume loss
 229 and no further investigation on this component is carried out. On the contrary, more than 95% of the
 230 total volume loss were from the components 2, 3 and 4 which are attributed to the volume of void
 231 between the excavated soil with the machine shield and the tunnel lining. One of the important factors
 232 that governs the magnitude of the components 2 and 3 during volume loss is the stand-up capabilities
 233 of the soil before the lining is installed and tail-void grouting is injected. It can be argued that for sandy
 234 soil, the stand-up capabilities mostly depend on the density and the degree of saturation of the soil. For
 235 saturated sands below the water table (as in this case study) the stand-up capability can be very limited.
 236 For component 4, the tail void grouting injection during the excavation to fill the void is of paramount
 237 important to reduce the collapse of the soil (Liu, C et al., 2020; Liu, X et al., 2019; Zheng et al., 2021).
 238
 239 **Figure 11** presents the measured volume of tail void grouting per ring in the EB and WB tunnels. The
 240 theoretical void volume between the excavation perimeter with the tunnel lining extrados, V_{void} , the
 241 design grout volume ($130\%V_{\text{void}}$), and the upper bound of volume $170\%V_{\text{void}}$ (Japan Society of Civil
 242 Engineers, 2016; Liu et al., 2019; Vonk, 2020) are depicted as the horizontal dotted line, the solid line
 243 and the dashed line, respectively.

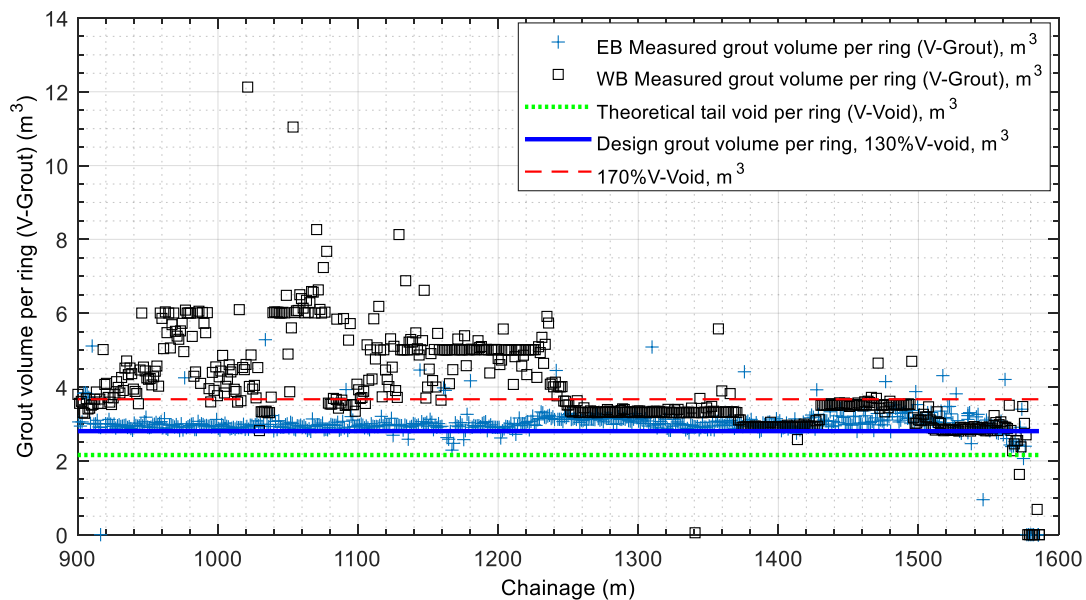


Figure 11. The measured volume of tail void grouting during the tunnel construction.

244

245 DISCUSSION

246 For the EB tunnel route, where most of the TBM excavated through the medium dense to dense sandy
 247 soil, AS2, the majority of tail void grout volume was approximate the design grout volume 130%V-void
 248 and less than 170%V-void. This is in line with the observations reported by previous research (Japan
 249 Society of Civil Engineers, 2016; Liu et al., 2017; Vonk, 2020) and resulted in small volume losses for
 250 most of monitoring sections on the EB tunnel route.

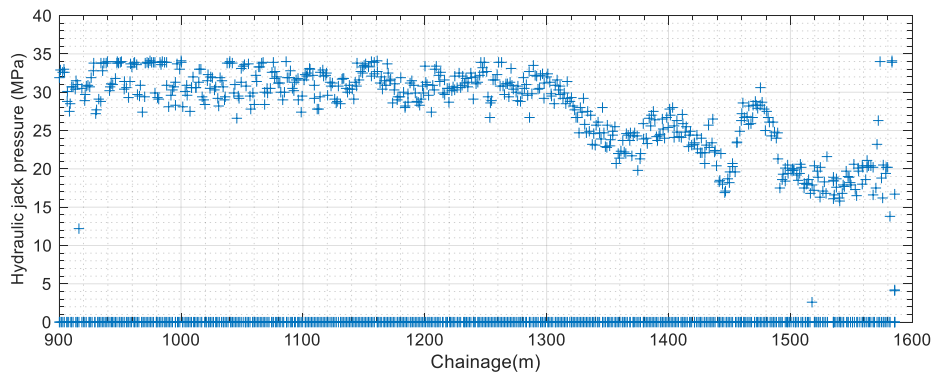
251 However, for WB tunnel route which excavated through the very loose to loose sandy soil, AS1, the tail
 252 void grout volume exceeded the values of 170%V-void from chainage 920m to 1240m, and sometimes,
 253 reached values up to nearly 6 times the theoretical tail void V-void. Interestingly, despite the larger
 254 injected volume of tail void grout (**Figure 11**), the volume losses at those locations were significantly
 255 larger than that at other locations in the WB tunnel route and EB tunnel route (**Figure 9b**). There are
 256 two possible reasons for this observation considered below.

257 The first reason was the very loose to loose, fully saturated, sandy soils AS1, might have been weakened
 258 by the prior EB tunnel excavation, allowed greater infiltration of tail void grout. This might have reduced
 259 the support effectiveness of the grout within the annulus between the lining extrados and the excavated
 260 ground for which it was designed.

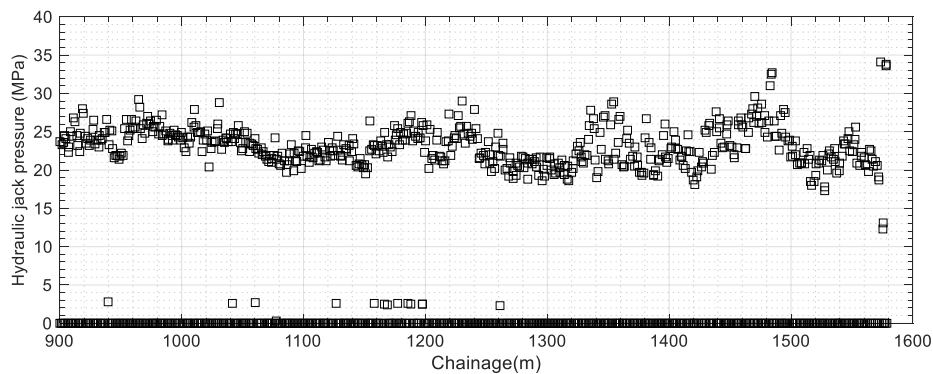
261 The second reason was that the cyclic loading from the hydraulic jacks thrusting the TBM forward during
 262 the excavation could have caused the cyclic changes in pore-water pressure, reducing the effective
 263 stress resulting in weakening and liquefaction of the soil. This, in turn, resulted in significantly larger

264 settlements and volume losses. As no measurements on pore-water pressure were carried out during
 265 the TBM driving, it is not possible to confirm whether liquefactions or soil loosening occurred. However,
 266 the pore-water pressure during the TBM driving can be estimated using the measured TBM face
 267 pressure, σ_F . When the TBM machine advances forward by the hydraulic jacks the excess pressure in
 268 the mixing chamber $\Delta\sigma_F$ is transferred to the pore-water pressure in front of the tunnel face. In the
 269 following analysis, it is assumed that $\Delta\sigma_F$ is initially supported by pore-water pressure before transferring
 270 to the surrounding soil skeleton (Knappett & Craig, 2019) during standstill and when the distance from
 271 the considered location to the TBM increases. As the soil is fully saturated, the excess pore pressure
 272 generated in front of the tunnel face, Δu , will be approximately equal to the change in the change in total
 273 stress, i.e. change in tunnel face pressure $\Delta\sigma_F$. This assumption may lead to an overestimation of Δu ,
 274 which is deemed reasonable for a conservative approach to assess liquefaction potential. **Figure 12 a,**
 275 **b** present the measured maximum and minimum hydraulic pressures in a single jack during the EB and
 276 WB tunnels for each lining ring. The corresponding measured tunnel face pressures are shown in
 277 **Figure 12 c, d.**

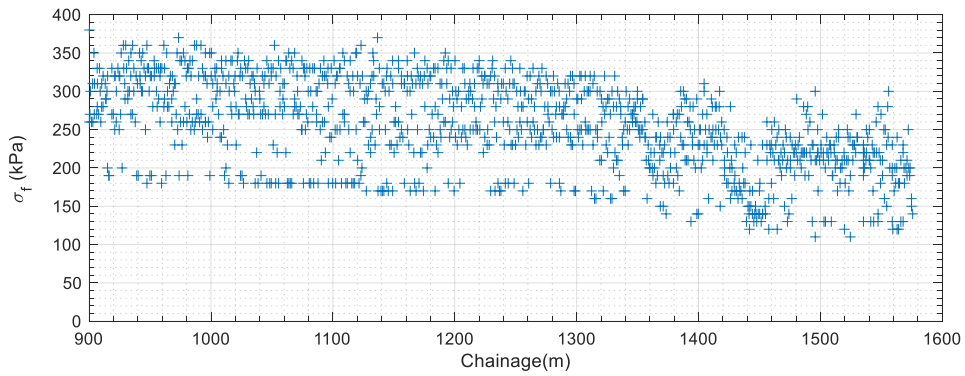
278
 279



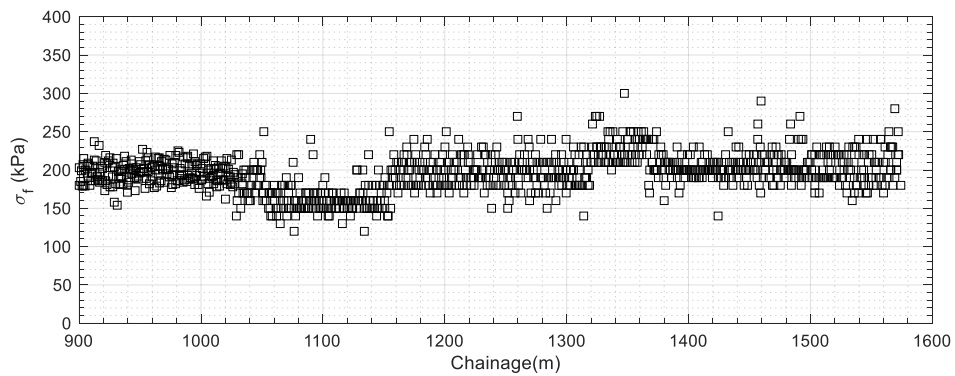
a. Measured hydraulic pressure in a jack during each ring in EB tunnel.



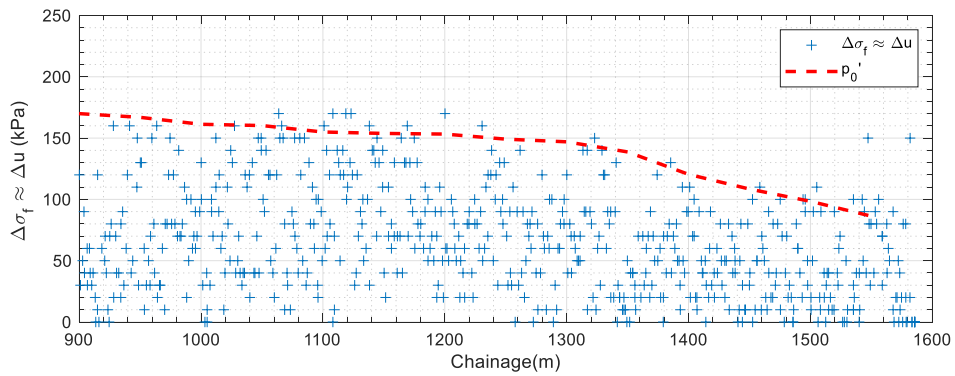
b. Measured hydraulic pressure in a jack during each ring in WB tunnel.



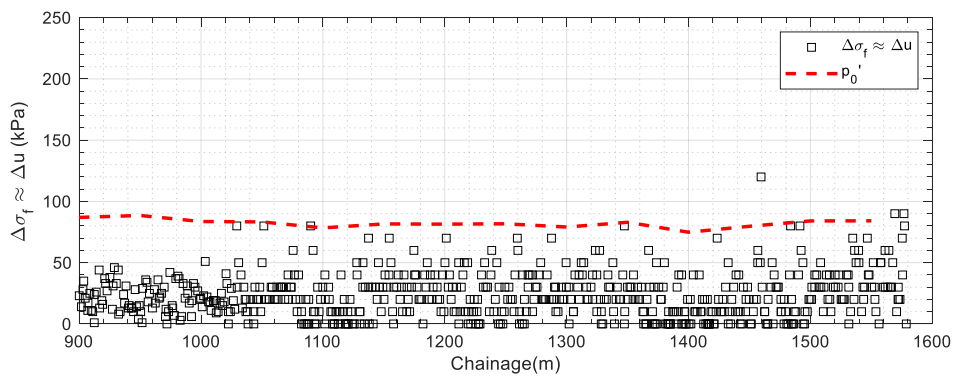
c. Measured tunnel face pressure σ_f during each ring in EB tunnel.



d. Measured tunnel face pressure σ_f during each ring in WB tunnel.



e. Changes in face pressure during each ring in EB tunnel.



f. Changes in face pressure during each ring in WB tunnel.

Figure 12. The TBM operational variables.

281 The maximum hydraulic pressures occur when all jacks thrust against the previously completed ring to
 282 advance the machine forwards. Then, during stoppage for the ring building, the jacks were sequentially
 283 retracted, by reducing their hydraulic pressure to zero, to allow for lining segment insertion. It is worth
 284 noting that other jacks remained pressurised to support the tunnel face and after the segment
 285 installation, the hydraulic pressure in the retracted jacks were increased again to allow for the retraction
 286 of other jacks for the new segment installation. Similar observations were reported by (Bezuijen et al.,
 287 2017; Yu et al., 2020).

288

289 The maximum hydraulic jack pressures for most of the rings in the EB tunnel were up to 34MPa which
 290 were larger than that of 30MPa for the WB tunnel (**Figure 12 a, b**). Due to the greater depth of the EB
 291 tunnel, hence greater friction and larger face pressure, a larger thrust was required. The effects of the
 292 hydraulic jack pressure were also reflected in **Figure 12 c, d, e** and **f** where the measured tunnel face
 293 pressures, σ_F , and the amplitude of the changes of the tunnel face pressure, $\Delta\sigma_F$, or the estimated
 294 excess pore pressure, Δu , in the EB tunnel was considerably larger than that for the WB tunnel. **Figure**
 295 **12 e, f** also present the initial mean effective stress p'_0 at the tunnel axis level z_0 .

$$p'_0 = \frac{\sigma'_{v0} + 2\sigma'_{h0}}{3} \quad (7)$$

$$\sigma'_{h0} = \sigma'_{v0}K_0 \quad (8)$$

296 where σ'_{v0} is the initial vertical effective stress at the tunnel axis level z_0 ;

297 σ'_{h0} is the initial horizontal effective stress at the tunnel axis level z_0 ;

298 K_0 is the earth pressure coefficient at rest (values of 0.503 to 0.552 were derived from the angle
 299 of friction obtained from laboratory tests).

300

301 It is worth noting that for both tunnels, some of the estimated Δu values approached the initial mean
 302 effective stress p'_0 (**Figure 12 e, f**) which is one of the indicators for liquefaction beside the liquefaction
 303 potential index, PL . The next section discusses in more detail the fundamentals of liquefaction in a critical
 304 state soil mechanics framework and analyses the relationship between the excess pore-water pressure
 305 Δu , liquefaction potential index, PL , with the tunnelling-induced volume loss, V_L .

306

307 THE EFFECTS OF LIQUEFACTION

308 Liquefaction can be caused by either flow or triggered by either monotonic or cyclic loading in undrained
 309 condition (Castro & Poulos, 1977; Hanzawa et al., 1979; Ishihara, 1993; Kramer, 1996; Poulos, 1981).

310 There are common conditions that facilitate the liquefaction reported in the literature. These conditions
 311 are coarse grained soil, loose state, high water table, high initial shear stress state, uniform grain size,
 312 large amount of round shape particles, small amount of fine particles. In soil mechanics, regardless of
 313 the total stress path, depending on the stress history and initial stress state of the soil, in undrained
 314 loading the typical effective stress path (**Figure 13**) follows one of three paths from the initial void ratio:
 315 (i) dense sand exhibits non flow hardening strain and approaches the steady state line (SSL) at large
 316 mean effective stress, p' , (Path A1-F, **Figure 13**) (ii) medium dense sand undergoes limited liquefaction
 317 behaviour by softening first then hardening (Path A2-E, **Figure 13**), (iii) loose and very loose sand shows
 318 the softening response to the state of very low effective mean stress, p' , near the origin of the q - p' plane
 319 (Path A3-B-C for monotonic load or path A3-D-C for cyclic loading, **Figure 13**). The equation for
 320 deviatoric stress q is presented below;

$$q = \sigma'_v - \sigma'_h \quad (9)$$

321 In the case of cyclic loading, the cyclic load brings the soil to the unstable state (flow liquefaction surface,
 322 FLS) then the effective stresses p' & q drop instantly as under static monotonic loading (Path A3-D-C,
 323 **Figure 13**). Therefore, the FLS is a reliable predictor for onset of flow liquefaction (Najma & Latifi, 2017).

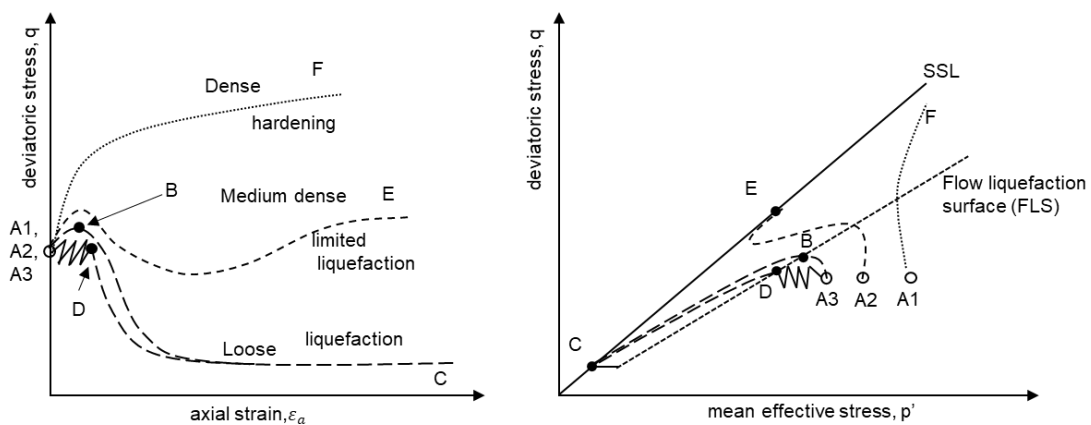


Figure 13. Dilation of dense sand, limited flow liquefaction of medium sand under monotonic loading and flow liquefaction of loose sand initiated by both monotonic and cyclic loading (After Kramer, 1996).

324
 325 Cyclic liquefaction can occur in a wide range of soil types and states of initial stress. In this case,
 326 contractive strain of the soil skeleton is accumulated after each loading-unloading cycle, accompanied
 327 by the pore-water pressure build-up, until large deformation is reached. Consequently, the effective
 328 stress path moves backward to the origin of the p' - q plane. At this unstable state of very low mean

329 effective pressure, a small disturbance can easily cause liquefaction (Ishihara et al., 1975; Seed & Lee,
330 1966; Vaid & Chern, 1983).

331

332 In this case study, the water table is approximately 2m below the ground surface. The soil profile along
333 the tunnel route includes the two low permeability clay layers AC2 and DC at the top and bottom
334 respectively. Therefore, for a conservative approach regarding liquefaction possibility, the two fully
335 saturated sandy soil layers in between can be considered as undrained when subjected to the cyclic
336 load from the tunnel driving. This is further confirmed by a long leakage length of 750m to 1000m
337 estimated by the approach suggested by Bezuijen (2017) and Bezuijen et al. (2017).

338

339 There have been several qualitative and quantitative methods to assess the liquefaction potential for
340 soils. One of the methods is to conduct advanced cyclic triaxial undrained tests to obtain required
341 parameters to establish the FLS (Najma & Latifi, 2017) as in **Figure 13**. Having the FLS allows the soil
342 at any stress state (p' , q), as such subjected to EPBM tunnelling, to be analysed for liquefaction potential.
343 However, such advanced cyclic triaxial tests were not conducted for the project reported in this case
344 study. There are, however, assessment methods for liquefaction potential that use commonly available
345 information such as the soil type, the geology profile and the SPT value, N (Matsuoka et al., 1993;
346 Tokimatsu & Yoshimi, 1983). The use of SPT for evaluation of liquefaction of soil was recommended by
347 previous research and professional bodies (Matsuoka et al., 1993; Railway Technical Research
348 Institute, 2012; New Zealand Geotechnical Society and Ministry for Business Innovation and
349 Employment, 2021; Tokimatsu & Yoshimi, 1983; Youd et al., 2001). The procedure suggested by
350 Iwasaki et al. (1984, 1981) was adopted to estimate liquefaction potential index, PL . This was done by
351 integration of factor of safety to liquefaction, FL , along the depth from the ground surface to the realistic
352 tunnel axis level, z_0 , instead of the conventionally accepted 20m depth as proposed by Iwasaki et al.
353 (1984, 1981) and Matsuoka et al. (1980) to take into account the position of tunnel that affects the ground
354 surface settlement. An example of the detailed calculation of PL is presented in the Appendix. **Figure**
355 **14** presents the relationship between the calculated PL with the corresponding volume losses at 14
356 locations which were within 20m from the nearest borehole.

357

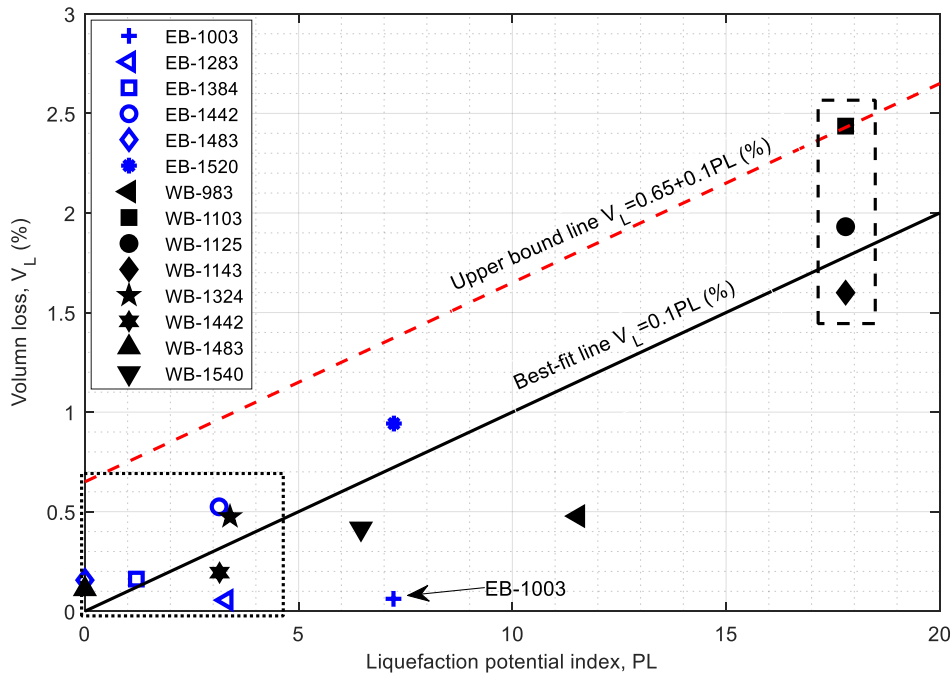


Figure 14. Relationship between the Liquefaction potential index, PL , and volume loss, V_L .

358

359 From **Figure 14**, it can be seen that the volume loss V_L and the liquefaction potential index PL are linearly
 360 proportional which can be described by the following equation;

$$V_L = 0.1PL(\%); \text{ with the mean square error } R^2 = 0.78 \quad (10)$$

361 Also in **Figure 14**, an upper bound line is suggested for prediction of volume loss from liquefaction
 362 potential index PL ;

$$V_L = 0.1PL + 0.65(\%); \quad (11)$$

363 For the largest volume losses ($V_L > 1.5\%$) at WB-1103, WB-1125 and WB-1143 (marked by the dashed
 364 box in **Figure 14**), these locations have the same characteristics including very high liquefaction
 365 potential index ($PL > 15$) and the estimated excess pore-water pressures, Δu , were close to or larger
 366 than the mean effective stress p'_0 (**Figure 12 f**) indicating that the stress path could have reached the
 367 flow liquefaction surface and the soil resistance dropped (Najma & Latifi, 2017). These two conditions
 368 imply a high possibility of liquefaction which might have loosened the sandy soil around the tunnel lining.
 369 That in turn led to excessive backfill grout permeation hence the reduction of the support effectiveness
 370 of the grout to the soils around the tunnel lining extrados. This explanation is corroborated by the high
 371 volume losses occurred along the tunnel shield and linings (components 2, 3 & 4 in **Figure 10**) and the
 372 abnormally large volume of tail void grouting at these locations (**Figure 11**).

373

374 For the sections with low Liquefaction potential index ($PL < 4$, marked by the dotted box in **Figure 14**)
375 the volume losses were generally less than 0.65% and are in line with the commonly observed volume
376 loss induced by TBM tunnelling and no further analysis is carried out. The anomalous data point EB-
377 1003 (annotated in **Figure 14**) is due to the EB tunnel lying in the dense sand AS2 meaning the cyclic
378 loading from TBM excavation attenuates through the dense sand layer and only caused negligible
379 impact to the sensitive loose sand layer AS1. The observation in the normal amount of volume of tail
380 void grouting in **Figure 11** supports this explanation.

381

382 **CONCLUSION**

383 EBPM tunnelling in saturated sandy soils inherently induces cyclic loads with associated changes in
384 pore-water pressure that may lead to liquefaction or soil loosening. This in turn, potentially, results in
385 large ground surface settlements. Therefore, through assessment of geotechnical data at local
386 boreholes, the use of a liquefaction potential index is recommended. In this research, despite the broad
387 variety of tunnel depths, thickness of soil layers, TBM operational variables, a reasonable relationship
388 between the liquefaction potential index, PL , and volume loss, V_L , (**Figure 14**) along the tunnel route
389 was found. Nevertheless, further research with more data from other projects is recommended to
390 corroborate this finding. **Equations 10** and **11** together with the calculation procedure in Appendix can
391 be useful when estimating where to expect the potential for large settlements caused by EBPM
392 tunnelling in sandy soil. For future tunnelling projects using EPBM in sandy soils, in additions to soil
393 parameters used in the Appendix, it is recommended that cyclic triaxial tests are conducted to gain a
394 better insight into soil behaviour under cyclic loading (Najma & Latifi, 2017). This would allow tunnelling
395 engineers to locate regions with high liquefaction potential index and estimate allowable excess pore-
396 water pressure to avoid liquefaction. Moreover, this would allow necessary soil reinforcement and/or
397 caution to be employed prior to tunnelling. Ground displacement monitoring, pore-water pressure
398 measurements are invaluable in assessing the liquefaction potential and adjusting the TBM operational
399 parameters if needed to ensure safe tunnelling.

400

401 **ACKNOWLEDGEMENT**

402 This research is funded by Vietnam National Foundation for Science and Technology Development
403 (NAFOSTED) under grant number 107.04-2020.31. This research was also supported by the Global
404 Challenges Research Funding provided by Research England.

405

406 **REFERENCES**

- 407 Aime, R., Aristaghes, P., Autuori, P., Minec, S., 2004. 15m diameter tunneling under Netherlands
408 polders, in: ITA World Tunnel Congress 2004-Underground Space for Sustainable Urban
409 Development.
- 410 Bezuijen, A., 2017. The influence of the leakage length on the initiation of backward erosion piping, in:
411 Proc. of the 25th Meeting of the European Working Group on Internal Erosion. Delft, the
412 Netherlands. pp. 88–96.
- 413 Bezuijen, A., 2006. Influence of pore pressure at tunnel face. *Tunnelling. A Decade of Progress.*
414 *GeoDelft 1995-2005* 277–284.
- 415 Bezuijen, A., Bakker, K.J., 2009. The influence of flow around a TBM machine, in: *Geotechnical*
416 *Aspects of Underground Construction in Soft Ground.* CRC Press, pp. 255–259.
- 417 Bezuijen, A., Bakker, K.J., 2007. Bentonite and grout flow around a TBM, in: ITA World Tunnel
418 Congress. pp. 383–388.
- 419 Bezuijen, A., Xu, T., Dias, T.G.S., 2017. Pore pressures in front of a slurry shield: development and
420 decline. *EURO:TUN 2017 - 4th International Conference on Computational Methods in Tunneling*
421 *and Subsurface Engineering.*
- 422 Biggart, A.R., Sternath, R., 1996. Storebaelt Eastern railway tunnel: construction, in: *Proceedings of*
423 *the Institution of Civil Engineers-Civil Engineering.* Thomas Telford-ICE Virtual Library, pp. 20–
424 39.
- 425 Broere, W., 2001. *Tunnel Face Stability & New CPT Applications (PhD Thesis).* Delft University of
426 Technology.
- 427 Castro, G., Poulos, S.J., 1977. Factors affecting liquefaction and cyclic mobility. *Journal of the*
428 *Geotechnical Engineering Division* 103, 501–516.
- 429 Chapman, D., Metje, N., Stärk, A., 2018. *Introduction to tunnel construction: Second edition,*
430 *Introduction to Tunnel Construction: Second Edition.* CRC Press.
431 <https://doi.org/10.1201/9781315120164>
- 432 Clough, G.W., Leca, E., 1993. EPB shield tunneling in mixed face conditions. *Journal of geotechnical*
433 *engineering* 119, 1640–1656.
- 434 Dias, T.G.S., Bezuijen, A., 2015. *TBM Pressure Models - Observations, Theory and Practice.* 15th
435 *Pan-American Conference on Soil Mechanics and Geotechnical Engineering - Geotechnical*
436 *Synergy in Buenos Aires 2015 - Invited Lectures* 347–374. [https://doi.org/10.3233/978-1-61499-](https://doi.org/10.3233/978-1-61499-599-9-347)
437 [599-9-347](https://doi.org/10.3233/978-1-61499-599-9-347)

438 Dimmock, P.S., 2003. Tunnelling-induced ground and building movement on the Jubilee Line
439 Extension (PhD thesis). University of Cambridge.

440 Do, N.A., Dias, D., Vu, T.T., Dang, V.K., 2021. Impact of the shield machine's performance
441 parameters on the tunnel lining behaviour and settlements. *Environ Earth Sci* 80, 1–13.
442 <https://doi.org/10.1007/S12665-021-09820-2>

443 Franza, A., Marshall, A.M., Zhou, B., 2019. Greenfield tunnelling in sands: The effects of soil density
444 and relative depth. *Geotechnique* 69, 297–307. <https://doi.org/10.1680/JGEOT.17.P.091>

445 Hanzawa, H., Itoh, Y., Suzuki, K., 1979. Shear characteristics of a quick sand in the Arabian Gulf.
446 *Soils and Foundations* 19, 1–15.

447 Ishihara, K., 1993. Liquefaction and flow failure during earthquakes. *Geotechnique* 43, 351–451.

448 Ishihara, K., Tatsuoka, F., Yasuda, S., 1975. Undrained deformation and liquefaction of sand under
449 cyclic stresses. *Soils and foundations* 15, 29–44.

450 Islam, M.S., Iskander, M., 2021. Twin tunnelling induced ground settlements: A review. *Tunnelling and*
451 *Underground Space Technology* 110, 103614. <https://doi.org/10.1016/J.TUST.2020.103614>

452 Iwasaki, T., Arakawa, T., Tokida, K.I., 1984. Simplified procedures for assessing soil liquefaction
453 during earthquakes. *International Journal of Soil Dynamics and Earthquake Engineering* 3, 49–
454 58. [https://doi.org/10.1016/0261-7277\(84\)90027-5](https://doi.org/10.1016/0261-7277(84)90027-5)

455 Iwasaki, T., Tokida, K., Tatsuoka, F., 1981. Soil liquefaction potential evaluation with use of the
456 simplified procedure, in: *International Conference on Recent Advances in Geotechnical*
457 *Earthquake Engineering and Soil Dynamics*, St. Louis. pp. 209–214.

458 Japan Society of Civil Engineers, 2016. Standard specifications for tunneling: Shield tunnel. Japan
459 Society of Civil Engineers Tokyo.

460 Jin, Dr.H., Yuan, Dr.D., Jin, Dr.D., Wu, Mr.J., Wang, Dr.X., Han, Dr.B., Mao, Dr.J., 2022. Shield
461 kinematics and its influence on ground settlement in ultra-soft soil: a case study in Suzhou.
462 <https://doi.org/10.1139/cgj-2021-0603>. <https://doi.org/10.1139/CGJ-2021-0603>

463 Jones, B.D., Clayton, C., 2013. Guidelines for Gaussian curve-fitting to settlement data. *Underground.*
464 *The Way to the Future* 645–652. <https://doi.org/10.1201/b14769-90>

465 Kaalberg, F.J., Ruigrok, J.A.T., de Nijs, R., 2014. TBM face stability & excess pore pressures in close
466 proximity of piled bridge foundations controlled with 3D FEM. *Geotechnical Aspects of*
467 *Underground Construction in Soft Ground* 555–560.

468 Kavvadas, M., Litsas, D., Vazaios, I., Fortsakis, P., 2017. Development of a 3D finite element model
469 for shield EPB tunnelling. *Tunnelling and Underground Space Technology* 65, 22–34.
470 <https://doi.org/10.1016/J.TUST.2017.02.001>

471 Knappett, J., Craig, R.F., 2019. *Craig's Soil Mechanics*. CRC Press.
472 <https://doi.org/10.1201/9781351052740>

473 Kramer, S.L., 1996. *Geotechnical earthquake engineering*. Pearson Education India.

474 Le, B.T., Kuriki, M., Phan, Q., Taylor, N., 2020. An empirical analysis on measured ground surface
475 settlement induced by TBM tunnelling in Ho Chi Minh city, *Lecture Notes in Civil Engineering*.
476 https://doi.org/10.1007/978-981-15-2184-3_38

477 Le, B.T., Nadimi, S., Goodey, R.J., Taylor, R.N., 2016. System to measure three-dimensional
478 movements in physical models. *Geotechnique Letters* 6. <https://doi.org/10.1680/jgele.16.00073>

479 Le, B.T., Nguyen, N.T., Divall, S., Goodey, R.J., Taylor, R.N., 2021. Modified gap method for
480 prediction of TBM tunnelling-induced soil settlement in sand-a case study, in: *Geotechnical*
481 *Aspects of Underground Construction in Soft Ground*. CRC Press, pp. 584–589.

482 Le, B.T., Taylor, R.N., 2018. Response of clay soil to three-dimensional tunnelling simulation in
483 centrifuge models. *Soils and Foundations* 58. <https://doi.org/10.1016/j.sandf.2018.03.008>

484 Leca, E., New, B., Reporter, G., 2007. Settlements induced by tunneling in Soft Ground. *Tunnelling*
485 *and Underground Space Technology* 22, 119–149. <https://doi.org/10.1016/j.tust.2006.11.001>

486 Liu, C., Cui, J., Zhang, Z., Liu, H., Huang, X., Zhang, C., 2021. The role of TBM asymmetric tail-
487 grouting on surface settlement in coarse-grained soils of urban area: Field tests and FEA
488 modelling. *Tunnelling and Underground Space Technology* 111.
489 <https://doi.org/10.1016/J.TUST.2021.103857>

490 Liu, C., Li, J., Zhang, Z., Li, P., Cui, J., Liu, H., Yang, Y., 2020. Model tests on tail-grouting process
491 during URUP shield tunneling in soft soil. *Tunnelling and Underground Space Technology* 103,
492 103451. <https://doi.org/10.1016/j.tust.2020.103451>

493 Liu, C., Zhang, Z., Regueiro, R.A., 2014. Pile and pile group response to tunnelling using a large
494 diameter slurry shield-Case study in Shanghai. <https://doi.org/10.1016/j.compgeo.2014.03.006>

495 Liu, C., Zhang, Z.X., Kwok, C.Y., Jiang, H.Q., Teng, L., 2017. Ground Responses to Tunneling in Soft
496 Soil Using the URUP Method. *Journal of Geotechnical and Geoenvironmental Engineering* 143,
497 04017023. [https://doi.org/10.1061/\(asce\)gt.1943-5606.0001695](https://doi.org/10.1061/(asce)gt.1943-5606.0001695)

498 Liu, X., Wang, F., Huang, J., Wang, S., Zhang, Z., Nawnit, K., 2019. Grout diffusion in silty fine sand
499 stratum with high groundwater level for tunnel construction. *Tunnelling and Underground Space*
500 *Technology* 93, 103051. <https://doi.org/10.1016/J.TUST.2019.103051>

501 Mair, R.J., 2008. Tunnelling and geotechnics: New horizons. *Geotechnique* 58, 695–736.
502 <https://doi.org/10.1680/geot.2008.58.9.695>

503 Mair, R.J., Taylor, R.N., 1997. Bored tunnelling in the urban environment, in: Fourteenth International
504 Conference on Soil Mechanics and Foundation Engineering. 14th ICSMGE (Hamburg)
505 Conference 19. Vol 4, pp. 2353–2380.

506 Matsuoka, M., Midorikawa, S., Wakamatsu, K., 1993. Liquefaction potential mapping for large area
507 using the digital national land information. *Journal of Structural and Construction Engineering*
508 (Transactions of AIJ) 452, 39–45. https://doi.org/10.3130/AIJSX.452.0_39

509 Najma, A., Latifi, M., 2017. Predicting flow liquefaction, a constitutive model approach. *Acta Geotech*
510 12, 793–808. <https://doi.org/10.1007/s11440-016-0517-x>

511 New Zealand Geotechnical Society, Ministry for Business Innovation and Employment, 2021.
512 Earthquake geotechnical engineering practice, Module 3: Identification, assessment and
513 mitigation of liquefaction hazards.

514 Nyren, R.J., 1998. Field measurements above twin tunnels in London Clay (PhD thesis). Imperial
515 College London.

516 O'Reilly, M.P., New, B.M., 1982. Settlements above tunnels in the United Kingdom - their magnitude
517 and prediction., in: *Tunnelling '82. Papers Presented at the 3rd International Symposium*. pp.
518 173–181.

519 Peck, R.B., 1969. Deep excavations and tunneling in soft ground. *Proc. 7th ICSMFE* 225–290.

520 Poulos, S.J., 1981. The steady state of deformation. *Journal of the Geotechnical Engineering Division*
521 107, 553–562.

522 Railway Technical Research Institute, 2012. Design standards for railway structures and commentary
523 (seismic design) (In Japanese).

524 Schmidt, B., 1969. Settlements and ground movements associated with tunneling in soil (PhD thesis).
525 University of Illinois.

526 Seed, H.B., Lee, K.L., 1966. Liquefaction of saturated sands during cyclic loading. *Journal of the Soil*
527 *Mechanics and Foundations Division* 92, 105–134.

528 Shi, J., Wang, F., Zhang, D., Huang, H., 2021. Refined 3D modelling of spatial-temporal distribution of
529 excess pore water pressure induced by large diameter slurry shield tunneling. *Comput Geotech*
530 137, 104312. <https://doi.org/10.1016/j.compgeo.2021.104312>

531 Shirlaw, J.N., 2016. Pressurised TBM tunnelling in mixed face conditions resulting from tropical
532 weathering of igneous rock. *Tunnelling and Underground Space Technology* 57, 225–240.
533 <https://doi.org/10.1016/J.TUST.2016.01.018>

534 Shirlaw, J.N., Ong, J.C.W., Rosser, H.B., Tan, C.G., Osborne, N.H., Heslop, P.E., 2003. Local
535 settlements and sinkholes due to EPB tunnelling. *Proceedings of the Institution of Civil Engineers*
536 - *Geotechnical Engineering* 156, 193–211. <https://doi.org/10.1680/geng.2003.156.4.193>

537 Standing, J.R., Selemetas, D., 2013. Greenfield ground response to EPBM tunnelling in London Clay.
538 *Géotechnique* 63, 989–1007. <https://doi.org/10.1680/geot.12.P.154>

539 Sugiyama, T., Hagiwara, T., Nomoto, T., Nomoto, M., Ano, Y., Mair, R.J., Bolton, M.D., Soga, K.,
540 1999. Observations of Ground Movements during Tunnel Construction by Slurry Shield Method
541 at the Docklands Light Railway Lewisham Extension-East London. *Soils and Foundations*.
542 https://doi.org/10.3208/sandf.39.3_99

543 Tatsuoka, F., Iwasaki, T., Tokida, K. ichi, Yasuda, S., Hirose, M., Imai, T., Kon-no, M., 1980. Standard
544 penetration tests and soil liquefaction potential evaluation. *Soils and Foundations* 20, 95–111.
545 https://doi.org/10.3208/SANDF1972.20.4_95

546 The British Tunnelling Society and The Institution of Civil Engineers, 2005. *Closed-Face Tunnelling*
547 *Machines and Ground Stability*.

548 Tokimatsu, K., Yoshimi, Y., 1983. Empirical Correlation of Soil Liquefaction Based on SPT N-Value
549 and Fines Content. *Soils and Foundations* 23, 56–74.
550 https://doi.org/10.3208/SANDF1972.23.4_56

551 Tóth, Á., Gong, Q., Zhao, J., 2013. Case studies of TBM tunneling performance in rock-soil interface
552 mixed ground. *Tunnelling and Underground Space Technology* 38, 140–150.
553 <https://doi.org/10.1016/j.tust.2013.06.001>

554 Vaid, Y.P., Chern, J.-C., 1983. Effect of static shear on resistance to liquefaction. *Soils and*
555 *foundations* 23, 47–60.

556 Vergara, I.M., Saroglou, C., 2017. Prediction of TBM performance in mixed-face ground conditions.
557 *Tunnelling and Underground Space Technology* 69, 116–124.
558 <https://doi.org/10.1016/j.tust.2017.06.015>

559 Vonk, M., 2020. Grouting the tail void (Master thesis). Delft University of Technology.

560 Vu, M.N., Broere, W., Bosch, J., 2016. Volume loss in shallow tunnelling. *Tunnelling and Underground*
561 *Space Technology* 59, 77–90. <https://doi.org/10.1016/J.TUST.2016.06.011>

562 Wan, M. S.P., Standing, J.R., Potts, D.M., Burland, J.B., 2017a. Measured short-term ground surface
563 response to EPBM tunnelling in London Clay. *Geotechnique* 67, 420–445.
564 <https://doi.org/10.1680/jgeot.16.P.099>

565 Wan, M.S.P, Standing, J.R., Potts, D.M., Burland, J.B., 2017b. Measured short-term subsurface
566 ground displacements from EPBM tunnelling in London Clay. *Géotechnique* 67, 748–799.
567 <https://doi.org/https://doi.org/10.1680/jgeot.SIP17.P.148>

568 Wan, M.S.P., Standing, J.R., Potts, D.M., Burland, J.B., 2019. Pore water pressure and total horizontal
569 stress response to EPBM tunnelling in London Clay. *Geotechnique* 69, 434–457.
570 <https://doi.org/10.1680/JGEOT.17.P.309>

571 Wongsaroj, J., Borghi, F.X., Soga, K., Mair, R.J., Sugiyama, T., Hagiwara, T., Bowers, K.H., 2006.
572 Effect of TBM driving parameters on ground surface movements: Channel Tunnel Rail Link
573 Contract 220, in: *Geotechnical Aspects of Underground Construction in Soft Ground*. London:
574 Taylor & Francis Group, pp. 335–341.

575 Xu, T., Bezuijen, A., 2019. Bentonite slurry infiltration into sand: Filter cake formation under various
576 conditions. *Geotechnique* 69, 1095–1106. <https://doi.org/10.1680/jgeot.18.P.094>

577 Xu, T., Bezuijen, A., 2018. Analytical methods in predicting excess pore water pressure in front of
578 slurry shield in saturated sandy ground. *Tunnelling and Underground Space Technology* 73,
579 203–211. <https://doi.org/10.1016/j.tust.2017.12.011>

580 Youd, T.L., Idriss, I.M., Andrus, R.D., Arango, I., Castro, G., Christian, J.T., Dobry, R., Finn, W.D.L.,
581 Leslie F. Harder, Jr., Hynes, M.E., Ishihara, K., Koester, J.P., Liao, S.S.C., William F. Marcuson,
582 I., Martin, G.R., Mitchell, J.K., Moriwaki, Y., Power, M.S., Robertson, P.K., Seed, R.B., Kenneth
583 H. Stokoe, I., 2001. Liquefaction Resistance of Soils: Summary Report from the 1996 NCEER
584 and 1998 NCEERNSF Workshops on Evaluation of Liquefaction Resistance of Soils. *Journal of*
585 *Geotechnical and Geoenvironmental Engineering* 127, 817–833.
586 [https://doi.org/10.1061/\(ASCE\)1090-0241\(2001\)127:10\(817\)](https://doi.org/10.1061/(ASCE)1090-0241(2001)127:10(817))

587 Yu, H., Mooney, M., Bezuijen, A., 2020. A simplified excavation chamber pressure model for EPBM
588 tunneling. *Tunnelling and Underground Space Technology* 103, 103457.
589 <https://doi.org/10.1016/J.TUST.2020.103457>

590 Zheng, D., Bezuijen, A., Thewes, M., 2021. An experimental study on foam infiltration into saturated
 591 sand and its consequence for EPB shield tunneling. *Tunnelling and Underground Space*
 592 *Technology* 111. <https://doi.org/10.1016/J.TUST.2021.103878>

593

594 **LIST OF FIGURES**

595 Figure 1. Idealisation of tunnelling induced soil displacement (after Le & Taylor, 2018). 3
 596 Figure 2. Ground surface settlement trough. 4
 597 Figure 3. Main components of Earth pressure balance tunnelling machine (Chapman et al., 2018). 6
 598 Figure 4. Measured excess pore pressure in front of a TBM in sandy soil (after Bezuijen, 2006). 7
 599 Figure 5. Illustration on components of volume loss (Wan et al., 2017b). 7
 600 Figure 6. Plan and longitudinal profile of the tunnel route. 9
 601 Figure 7. TBM advance rate. 10
 602 Figure 8. Ground surface settlement troughs and Gaussian approximations. 14
 603 Figure 9. Longitudinal ground surface settlement and volume loss. 15
 604 Figure 10. Typical normalised volume losses along the tunnel centre-line. 16
 605 Figure 11. The measured volume of tail void grouting during the tunnel construction. 17
 606 Figure 12. The TBM operational variables. 19
 607 Figure 13. Dilation of dense sand, limited flow liquefaction of medium sand under monotonic loading
 608 and flow liquefaction of loose sand initiated by both monotonic and cyclic loading (After Kramer, 1996).
 609 21
 610 Figure 14. Relationship between the Liquefaction potential index, PL, and volume loss, VL. 23

611

1 **APPENDIX – CALCULATION PROCEDURE FOR LIQUEFACTION POTENTIAL INDEX**

2 The liquefaction potential index, PL , can be calculated by weighted integration of the safety rate to
 3 liquefaction, F , with depth z as depicted in **Figure A1** and described by the Equation A.1 (Iwasaki et
 4 al., 1981, 1984);

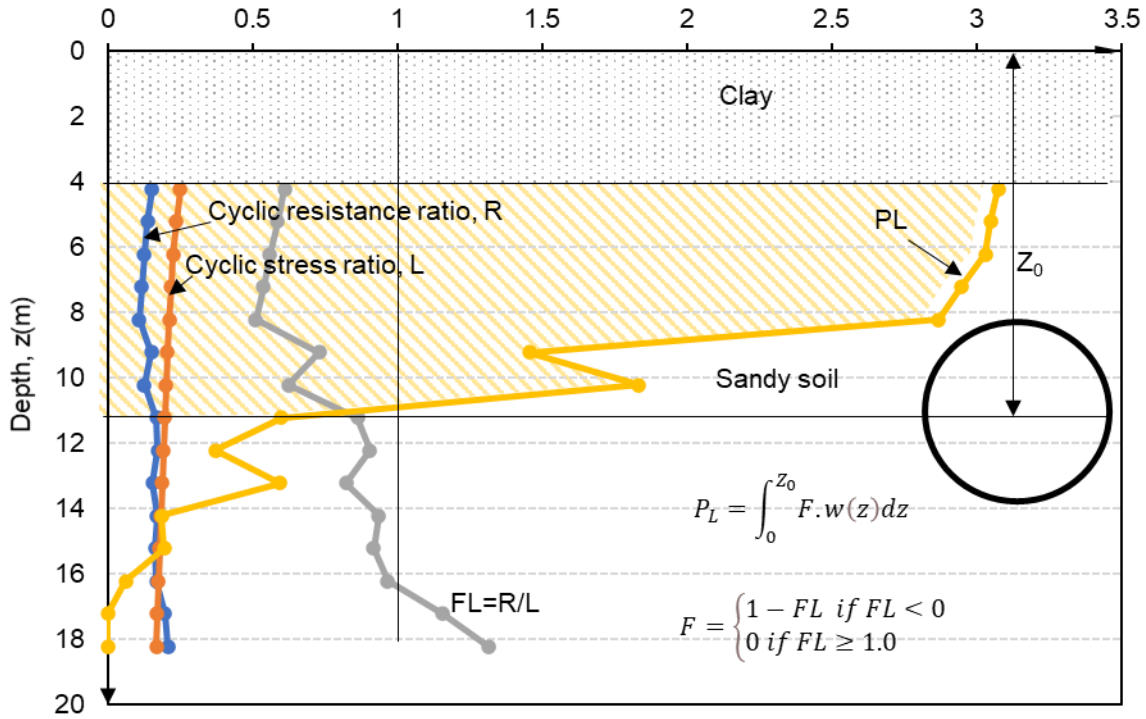


Figure A1. Definition of FL and PL

5

$$PL = \int_0^{z_0} F \cdot w(z) dz \quad (A.1)$$

6 Where $w(z)$: the weight function in accordance with depth z , larger weight is assigned for surficial
 7 upper depth;

$$w(z) = 10 - 0.5z \quad (A.2)$$

8 z : depth from the ground surface (m).

$$F = \begin{cases} 1 - FL & \text{if } FL < 0 \\ 0 & \text{if } FL \geq 1.0 \end{cases} \quad (A.3)$$

9 FL is the factor of liquefaction resistance;

$$FL = \frac{R}{L} \quad (A.4)$$

10 L is the seismic shear stress ratio;

$$L = \frac{\alpha}{g} \cdot \frac{\sigma_v}{\sigma'_v} \cdot \gamma_d \quad (\text{A.5})$$

11 where

12 α : peak ground acceleration, in the region of Ho Chi Minh city for sandy soil: $\alpha = 0.11448 g$

13 σ_v : vertical total stress (kN/m^2)

14 σ'_v : vertical effective stress (kN/m^2)

15 γ_d : reduction coefficient, $\gamma_d = 1 - 0.015z$, depth below ground level (m)

16 For the dynamic shear strength ratio R , there are several methods to determine R using different
 17 sets of geotechnical inputs. In this paper, the method suggested by (Iwasaki et al., 1981, 1984) is
 18 used and presented as below;

19 The dynamic shear strength ratio R is calculated with cyclic triaxial strength ratio R_L from following
 20 correction formula

$$R = C_w \cdot R_L \quad (\text{A.6})$$

21

22 Cyclic triaxial strength ratio R_L is defined experimentally from the following formula

$$R_L = \begin{cases} 0.0882\sqrt{N_a/1.7} & \text{if } N_a < 14 \\ 0.0882\sqrt{N_a/1.7} + 1.6 \times 10^{-6}(N_a - 14)^{4.5} & \text{if } 14 \leq N_a \end{cases} \quad (\text{A.7})$$

23 N_a : amended N-value taken into account the effect of grain size

24 For sandy soil, then N_a is calculated as:

$$N_a = C_1 N_1 + C_2 \quad (\text{A.8})$$

25 In which C_1 & C_2 are the coefficients considering the fine content F_c of the soil

$$C_1 = \begin{cases} 1.0 & \text{if } 0\% \leq F_c \leq 10\% \\ \frac{F_c + 40}{50} & \text{if } 10\% \leq F_c < 60\% \\ \left(\frac{F_c}{20}\right) - 1 & \text{if } 60\% \leq F_c \end{cases} \quad (\text{A.9})$$

$$C_2 = \begin{cases} 1.0 & \text{if } 0\% \leq F_c < 10\% \\ \frac{F_c - 10}{18} & \text{if } 10\% \leq F_c \end{cases} \quad (\text{A.10})$$

26

27 For gravelly soil:

$$N_a = \left[1 - 0.36 \log_{10} \left(\frac{D_{50}}{2} \right) \right] N_1 \quad (\text{A.11})$$

28

29 With D_{50} : mean grain diameter (mm)

30 Normalised N-value (N_1) for effective upper load pressure of $1 \text{ kgf/cm}^2 = 100 \text{ kPa}$ is given below.

$$N_1 = 1.7 \frac{N}{\sigma'_v / 100 + 0.7} \quad (\text{A.12})$$

31 N: raw SPT count at site

32 The coefficient C_w is defined according to the type of the seismic motion as follows.

33 a) Type 1: Seismic motion by great inter-plate earthquake with low occurrence frequency

34 Large amplitude acts for a long time repeatedly $C_w = 1.0$.

35 b) Type 2: Seismic motion by large inland earthquake with very low occurrence frequency

$$C_w = \begin{cases} 1.0 & (R_L \leq 0.1) \\ 3.3R_L + 0.67 & (0.1 < R_L \leq 0.4) \\ 2.0 & (0.4 < R_L) \end{cases} \quad (\text{A.13})$$

36 In this case study, the area is subjected to Type 2 hence C_w is estimated by equation A.13.

37 The PL results obtained from Iwasaki's method for boreholes a long WB tunnel is presented in

38 Table A1. The locations of the boreholes can be referred to **Figure 6** in the manuscript.

39 Table A1. PL results along the WB tunnel route.

Borehole	Chainage	PL
ABH-2	1000	11.5
U-160	1120	17.8
ABH-3	1300	3.4
U-170	1380	0.0
ABH-4	1440	3.2
LKH-4	1480	0.0
U-176	1540	6.5

40

41 In the manuscript, **Figure 14** uses the PL values from Table A1 for the monitoring sections that are
 42 within approximately 20m from the borehole.

43 For practical application, PL can be used as an indicator for the liquefaction potential as below;

- 44 $PL = 0$: Liquefaction potential is very low;
- 45 $0 < PL \leq 5$: Liquefaction potential is low;
- 46 $5 < PL \leq 15$: Liquefaction potential is high, caution should be taken during tunnel
47 excavation process;
- 48 $15 > PL$: Liquefaction potential is very high, caution should be taken during tunnel
49 excavation process.